Relocating operational and damaged bikes in free-floating systems
A data-driven modeling framework for level of service enhancement

Chang, Ximing; Wu, Jianjun; Sun, Huijun ; Correia , Gonçalo Homem de Almeida; Chen, JianHua

DOI
10.1016/j.tra.2021.09.010

Publication date
2021

Document Version
Accepted author manuscript

Published in
Transportation Research Part A: Policy and Practice

Relocating operational and damaged bikes in free-floating systems: A data-driven modeling framework for level of service enhancement

Ximing Chang[a], Jianjun Wu[a,b,*], Huijun Sun[c], Gonçalo H. A. Correia [d], Jianhua Chen[e]

[a] State Key Laboratory of Rail Traffic Control and Safety, Beijing Jiaotong University, Beijing, China

[b] Key Laboratory of Transport Industry of Big Data Application Technologies for Comprehensive Transport, Ministry of Transport, Beijing Jiaotong University, Beijing, China

[c] School of Traffic and Transportation, Beijing Jiaotong University, Beijing, China

[d] Department of Transport & Planning, Delft University of Technology, Delft, the Netherlands

[e] Shenzhen Polytechnic, Shenzhen, China

Abstract

Free-floating bike sharing is an innovative and sustainable travel mode, where shared bikes can be picked up and returned at any proper place on the streets and not just at docking stations. Nevertheless, in these systems, two major problems arise. One is the imbalance of free-floating shared bikes (FFSB) between zones due to one-way trips, the other is the damaged bikes that must be brought for repair. In this study, a modeling framework for dynamic relocating operational and damaged bikes is proposed that starts with predicting the number and location of shared bikes using deep learning algorithms. The demand forecasting model adopts the Encoder-Decoder architecture embedded with the attention mechanism to further enhance the model's prediction ability and flexibility. Then, a data-driven optimization model for FFSB relocations is presented, where the multi-period optimization is applied to dynamically plan the relocation activities throughout the day. A new hybrid metaheuristic algorithm that incorporates variable neighborhood search (VNS) and enhanced simulated annealing (ESA) algorithm is developed for solving the relocating problem, in which satisfactory performance is observed from the numerical example. We test the proposed framework with the real-world FFSB data from Beijing, China. The results show that relocating both operational and damaged bikes timely decreases the probability of users finding damaged bikes in the system, but leads to higher relocation costs. For peak-hours, considering only the operational bikes for relocation is the most effective strategy given the limited relocation resources. It is urgent at those times of the day to focus on providing bikes to clients where they are undersupplied.

Keywords: free-floating bike-sharing; demand forecasting; bike relocation; multi-period optimization; damaged bikes' collection.

* Corresponding author: jjwu1@bjtu.edu.cn (Jianjun Wu);

1. Introduction

Bike-sharing systems provide a mobility service where available bikes are adopted for shared use in a short time. Traditional station-based shared bikes should be parked at fixed docking stations and kiosk machines, which usually lead to complaints for being far away from the destination, or having no free parking spaces. Free-floating shared bike (FFSB) is an emerging travel mode in which shared bikes are approved to park almost everywhere in the street network. With the dramatic expansion of FFSBs, the crowded streets and insufficient public transit system can be relieved by offering a more flexible travel mode choice (Li et al., 2019; Ma et al., 2020). The door-to-door travel capability allows shared bikes to substitute cars on short-distance trips or to cover the last mile from the public transport stations to the final destination. Besides, FFSB is an environmentally-friendly transport mode, which produces no pollution during travel and makes contributions to the transition into a low-carbon and green society (Lin et al., 2018). The new generation of FFSB relies on mobile Internet and Global Positioning System (GPS), enabling bike use, payment, and data transmission at any time, from anywhere. Bike-sharing systems are popular in many cities around the world. For example, there were about 2.2 million bikes in the streets of Beijing, China in February 2018 (Sina, 2018), from which 62.90% of the customers were typically using shared bikes as a last-mile connection of public transport trips. Currently, the use of shared bikes soared in Beijing after the city lifted a lockdown due to the COVID-19 pandemic. Shared bikes provide a safe way to travel amid the epidemic because they pose a low risk of people getting infected with the virus compared to mass public transport such as the metro (China daily, 2020).

FFSBs provide seamless connections between various transportation modes (Ma et al., 2019). Nevertheless, some problems have arisen with the bike-sharing boom, such as a high number of damaged bikes and the crowded parking areas, sometimes leaving little space available for pedestrians to walk. In station-based bike-sharing systems, stations can have a deficit or surplus of bikes, or on few occasions being self-balanced. In the free-floating bike-sharing system, users have no need to worry about the problems of full stations since they can park anywhere. However, the spatial and temporal distribution of shared bikes can still be imbalanced, and it may be difficult to find available FFSBs near the trip origin during peak hours (Du et al., 2019). Furthermore, as FFSBs are scattered in different places and their positions may change among different zones at different time of day, the rebalancing operations can even be more challenging than that of the traditional station-based bike-sharing system (Caggiani et al., 2018). Besides, with the rapid growth of bike-sharing systems, vast piles of damaged bikes have been abandoned in the streets because of inadequate regulations and recycling plans. For example, the height of the seat may not be adjustable anymore, or the brakes may be malfunctioning, which greatly affects the user experience and adds a safety risk to the usage of such systems (Lu et al., 2019). Therefore, integrating the recycling of damaged bikes into the efficient relocation strategies of free-floating bike-sharing systems should be studied.

Essentially, there are two strategies for shared bike rebalancing (Laporte et al., 2018; Shui and Szeto, 2020). The first is a user-based rebalancing method (Pfrommer et al., 2014; Heitz, et al., 2018; Pan et al., 2019). In this strategy, users are encouraged

to pick up or return the shared bikes at feasible locations to balance the distribution in local areas. Pfrommer et al. (2014) designed a dynamically varying reward mechanism to encourage customers to park the shared bikes at nearby underused stations, thus reducing the expected costs of redistribution using dedicated staff. Pan et al. (2019) modeled the rebalancing problem in the dockless bike-sharing system in a Markov decision process. They developed a deep reinforcement learning algorithm to incentivize users to help rebalance the whole system. Results show that the proposed framework performs close to the 24-timeslot look-ahead optimization. The second is the operator-based rebalancing method in which the repositioning process is accomplished by employing relocation staff and vehicles to collect bikes from redundant stations and deliver them to stations with too few bikes. In real scenarios, ignoring the existing damaged bikes will affect the travel demand forecasting and rebalancing optimization (Alvarez-Valdes et al., 2016; Wang and Szeto, 2018; Du et al., 2020). If the damaged shared bikes stay in one zone without being collected, the staff may mistake them as operational shared bikes therefore no new bikes will be allocated to that zone. From the point of view of the users, after they scan the QR code to unlock a bike, they may find that it is unusable which delays their trips. The damaged bike not only affects the user's travel experience but also adds a safety problem that may only be identified later during the trip. Therefore, in the process of FFSB relocation, the damaged shared bikes should be collected and moved back to the depot directly for repair, while the operational bikes should be redistributed to the needed places.

The dynamic relocation of the FFSB should consider the three challenges: users' demand forecasting, loading quantity determination, and vehicle routing (Regue and Recker, 2014; Zhang et al., 2017; Legros, 2019). The fluctuating spatial and temporal travel demand of FFSBs can be considerable, which will potentially exacerbate the imbalance between supply and demand in the absence of timely relocation strategies. For this reason, accurately predicting the usage of FFSBs provides useful information for rebalancing and improves the operational efficiency of the bike-sharing systems (Caggiani, et al., 2018; Xu et al. 2018). In recent years, deep learning has developed rapidly for more complex predicting tasks. Artificial intelligence (AI) algorithms have been adopted for travel demand forecasting such as Recurrent Neural Network (RNN) and Long Short-Term Memory (LSTM) network. Thus, the spatiotemporal characteristics of bike-sharing demand can potentially be captured to improve prediction accuracy (Liu et al., 2019; Hao et al., 2019). The data-driven method integrates data collection, analysis, and modeling in a whole continuous process. The decisions are made based on the insights derived from actual data rather than intuition or apriori normative concepts of optimality. The data-driven modeling makes no strict assumptions on the structure of the data (Solomatine and Ostfeld, 2008; Huo et al., 2020). Through continuous data collection and updating of shared bike travel records, useful information for dynamic relocation can be derived. Data-driven modeling helps to use historical information to predict the future demand and assign relocation tasks using the forecasted demand, which avoids performing on false assumptions and biases.

This paper proposes a comprehensive data-driven bike relocation optimization method with both operational and damaged FFSB. The whole method contains three parts: FFSB travel demand prediction, the relocation needs determination, and the data-driven relocation. To summarize, the main contributions of this paper are the following:

- We establish a novel attention-based passenger flow (ATTPF) predicting model to forecast the short-term inflow and outflow of FFSB, which adopts the Encoder-Decoder architecture embedded with the attention mechanism to enhance the model's prediction ability and flexibility.
- Based on the predicted demand gap, we propose a data-driven optimization model for bike-sharing relocation that considers the damaged bikes' collection. The multi-period optimization is applied to handle the time-varying relocation demand. The number of damaged shared bikes is detected based on the users' travel behavior using the historical travel records data.
- We develop a new hybrid metaheuristic algorithm that incorporates variable neighborhood search (VNS) and the enhanced simulated annealing (ESA) algorithm to solve the large-scale real-word FFSB system in Beijing, China.

The remainder of this paper is organized as follows. Section 2 reviews the literature regarding short-term bike demand prediction and bike-sharing relocation. Section 3 describes the whole framework and the methodology behind each model. Section 4 provides the data description and analysis. We evaluate our method with real-world cases and discuss the results in Section 5. Finally, conclusions are drawn in Section 6.

2. Literature review

2.1. Studies regarding short-term bike demand prediction

Bike-sharing systems suffer from the effects of fluctuating spatiotemporal travel demand that leads to inefficient relocation service and high operating costs. On the one hand, the shortage of shared bikes contributes to hinder the usage of bikes. On the other hand, if there are too many bikes in the system, the unused bikes may occupy a lot of public space and increase the costs for the bike company unnecessarily. Therefore, dynamic bike-sharing rebalancing contributes to the management of these systems, where accurately forecasting the demand is the fundamental component (Sohrabi et al., 2020; Shui and Szeto, 2020; Chang et al., 2021).

In the previous literature, the short-term demand prediction for bikes is based on classic statistical methods, including Autoregressive Integrated Moving Average (ARIMA) and its variants (Yoon et al., 2012). In recent years, thanks to massive travel mobility data and higher computing power, it is possible to uncover the dynamic characteristics in the transportation system with more data-driven advanced techniques. Some machine learning models, including Random Forest (RF), Support Vector Machine (SVM), and neural network models have been widely used in shared bike travel demand forecasting (Ashqar et al., 2017; Fournier et al., 2017; Wang and Kim, 2018). Ashqar et al. (2017) modeled the available shared bikes at stations using Random Forest (RF) and Least-Squares Boosting (LSBoost) algorithms in San Francisco. Results showed that spatially correlated stations and the prediction horizon time were significant predictors. Fournier et al. (2017) estimated the seasonal bike usage patterns with a sinusoidal model, which was able to capture average daily travel demand on the

monthly and annual scale. Although machine learning models can efficiently identify temporal trends and patterns for short-term passenger flow prediction, these models lack the interpretation of predicting results due to their "black-box" nature.

Deep learning methods have also been introduced for bike-sharing travel demand prediction. Different deep neural network structures can effectively extract the spatial and temporal features of travel needs and improve prediction accuracy. Xu et al. (2018) forecasted the dynamic FFSB demand with the deep learning algorithms, where LSTM was used to predict the short-term trip production and attraction at different traffic analysis zones. Lin et al. (2018) predicted hourly demand in a dock-based bike-sharing network based on the graph convolutional network (GCN), which can effectively learn hidden correlations between stations. In the neural network training process, the model may fail to memorize all the input features, which will degrade its performance. The intervention of an attention mechanism enables the model to pay particular attention to specific parts of the relevant input variables while ignoring others in deep neural networks. He et al. (2020) studied the flow prediction for bike-sharing stations using graph attention convolutional neural networks. The syncretic attention mechanisms captured and differentiated station-to-station correlations, and thus improved the model's accuracy and robustness.

2.2. Studies regarding operator-based bike-sharing relocations

In operator-based bike-sharing relocations, the operators drive the relocation vehicles to rebalance shared bikes across different stations to satisfy the users' demand. Laporte et al. (2018) surveyed the main operational research issues arising in shared mobility systems, including the station location problem, the station inventory problem, and the vehicle repositioning problem. Shui and Szeto (2020) reviewed the papers on bicycle-sharing service planning problems. They emphasized that the users' demand forecasting, loading determination, and vehicle routing should be considered in a dynamic bicycle repositioning operation. In Table 1, we summarize the scientific publications regarding operator-based bike-sharing relocation according to the relocation demand determination, objectives, solution algorithms, and whether the damaged bikes are considered or not.

The FFSB rebalancing problem can be modeled in a static or a dynamic approach. The static rebalancing is performed with a predetermined schedule by staff, while users cannot act on the bikes during the rebalancing task. This process is usually carried out during the night when the number of users is lower. Liu et al. (2018) studied the bike-sharing rebalancing problem with heterogeneous vehicle fleets, where the relocation vehicles were allowed to visit the stations multiple times. Usama et al. (2020) formulated the static bike-sharing rebalancing operation while simultaneously considering faulty bikes. Numeric examples show that with the increase of faulty bikes in the network, the rebalancing trucks have to travel longer paths and make more space for the faulty bikes. Dynamic rebalancing occurs during daytime taking into account what is happening in real-time with the demand changes. Zhang et al. (2017) formulated the dynamic repositioning of shared bikes as a time-space network flow model, where the user dissatisfaction forecasting, the vehicle routing, and the bicycle repositioning are considered. Caggiani et al. (2018) forecasted the trend on available bikes in each spatio-temporal zone and then presented a decision support system for the dynamic

real-time bike redistribution. To handle the time-varying demand, Shui and Szeto (2018) proposed a framework for the dynamic green bike repositioning, where the dynamic problem is decomposed into several static sub-problems by the rolling horizon approach.

In the previous bike-sharing rebalancing research, the objective functions include: minimizing total travel cost (Dell'Amico et al., 2014), minimizing the total travel duration (Angeloudis et al., 2014), minimizing the total demand dissatisfaction (Szeto and Shui, 2018), etc. Wang and Szeto et al. (2018) relocated both operational and broken bikes in a bike-sharing network to achieve a perfect balance between bike demand and supply with the object of minimizing the total CO2 emissions of all the vehicles. Multi-objective models have also been proposed in bike-sharing rebalancing studies focusing on real-world problems. Usama et al. (2019b) built a mixed-integer linear program to minimize the user's dissatisfaction, the vehicle routing cost, and the vehicle waiting time simultaneously. For large-scale bike-sharing programs, different algorithms are adopted to obtain both effective and efficient solutions, such as an iterated tabu search (Ho and Szeto, 2014), a branch-and-bound algorithm (Kadri et al., 2016), a large neighborhood search method (Ho and Szeto, 2017; Pal et al., 2017), an enhanced chemical reaction optimization (Szeto et al., 2016; Liu et al., 2018), an enhanced artificial bee colony algorithm (Shui and Szeto, 2018) and a greedy-genetic heuristic (Du et al., 2020), etc.

So far, it is possible to say that there have been several breakthroughs and innovations in the methods for solving the bike-sharing rebalancing problem. However, some issues remain. Firstly, most of the studies are based on station-based bike-sharing systems. But emerging FFSBs are developing rapidly and massive data can be recorded by built-in GPS to reflect the user's travel mobility patterns. Besides, modeling in a data-driven approach considers the time-dependent demand, where the updated data from the current period will join the historical dataset to derive new statistics. Secondly, it is necessary to consider the damaged bikes during the dynamic relocating process since this is a phenomenon that decreases the quality of service and overall experience in using bike-sharing schemes. Without effective relocation operations, the damaged shared bikes are abandoned on the streets and lead to more traffic congestion, which is a huge waste of resources. Besides, riding potentially damaged bikes is unsafe, and all these hazards can cause crashes. Operational bikes are needed to be redistributed among zones to satisfy the users' travel demand while the damaged bikes should be collected and carried back to the depot for repair. Thirdly, the dynamic rebalancing problem depends highly on the accurate prediction of the usage of the system (Caggiani et al., 2018). New forecasting algorithms in deep learning can capture the fluctuating spatial and temporal characteristics of travel demand, which provides useful information for rebalancing the system, therefore, improving users' experience and allowing better management of the system.

Table 1. Research on the operator-based bike-sharing relocation problem in the literature.

References	Bike type [a]	Relocation Pattern	Relocation demand	Objective	Damaged bikes	Solution method
Dell'Amico et al.(2014)	SBSB	Static	Given	Minimize total travel cost	No	Branch-and-cut algorithm
Alvarez-Valdes et al. (2016)	SBSB	Static	A decision variable	Minimize the weighted sum of the total unsatisfied demand and the number of relocated vehicle	Yes	A heuristic algorithm based on minimum cost flow problem and an insertion algorithm
Szeto et al. (2016)	SBSB	Static	Given	Minimize the weighted sum of unmet demand and vehicle's operational time	No	Enhanced chemical reaction optimization
Ho and Szeto et al. (2017)	SBSB	Static	A decision variable	Minimize total penalty cost and the weighted total travel time	No	A hybrid large neighborhood search
Wang and Szeto et al. (2018)	SBSB	Static	A decision variable	Minimize the total CO2 emissions of all the vehicles	Yes	The clustering method and CPLEX
Regue et al. (2014)	SBSB	Dynamic	Predicted by gradient boosting machines	Maximize the weighted sum of utility gained	No	Traditional commercial solvers
Zhang et al. (2017)	SBSB	Dynamic	Predicted by continuous-time Markov chain	Minimize the total expected user dissatisfaction	No	A heuristic algorithm based on the column generation
Shui and Szeto (2018)	SBSB	Dynamic	Given in a rolling horizon approach	Minimize the total unmet demand and the fuel and CO2 emission cost of the repositioning vehicle	No	An enhanced artificial bee colony algorithm
Pal et al. (2017)	FFSB	Static	Given	Minimize the make-span of the rebalancing fleet	No	Large neighborhood search
Liu et al. (2018)	FFSB	Static	A decision variable	Minimize the weighted sum of the inconvenience level	No	Enhanced chemical reaction optimization
Sun et al. (2019)	FFSB	Static	Given	Maximize the user satisfied demand	No	The clustering algorithm and Branch-and-cut algorithm
Usama et al. (2019a)	FFSB	Static	Given	Minimize the total cost of vehicle routing	Yes	Branch-and-cut algorithm
Usama et al. (2019b)	FFSB	Static	Given	Minimize the user's dissatisfaction, the vehicle routing cost, and the vehicle waiting time	Yes	Branch-and-cut algorithm
Du et al. (2020)	FFSB	Static	Given	Minimize the total repositioning time	Yes	Greedy-genetic heuristic
Usama et al. (2020)	FFSB	Static	Given	Minimize the user dissatisfaction, rebalancing routing cost and handling length of faulty bikes	Yes	Branch-and-cut algorithm
Caggiani et al. (2018)	FFSB	Dynamic	Predicted by artificial neural networks	Minimize the total travel time	No	Spatio-temporal clustering based algorithm
Zhai et al. (2019)	FFSB	Dynamic	Markov chain process	Minimize the rebalancing cost	No	Branch-and-cut algorithm
Barabonkov et al. (2020)	FFSB	Dynamic	Poisson process	Minimize the lost demand	No	Branch-and-cut algorithm
This paper	**FFSB**	**Dynamic**	**Predicted by ATTPF model**	**Minimize the total relocation cost**	**Yes**	**A hybrid metaheuristic algorithm with variable neighborhood search and enhanced simulated annealing**

[a] SBSB: station-based shared bikes; FFSB: free-floating shared bikes.

3. Methodology

In this paper, we propose a new comprehensive data-driven bike relocation framework with both operational and damaged FFSBs in Fig.1. The whole framework includes the FFSB travel demand prediction, the relocation needs determination, and the data-driven relocation. The framework starts with the prediction of the number and position of shared bikes over a system operating area and ends with the relocation route decision. The multi-period optimization approach is applied to dynamically plan the relocation activities.

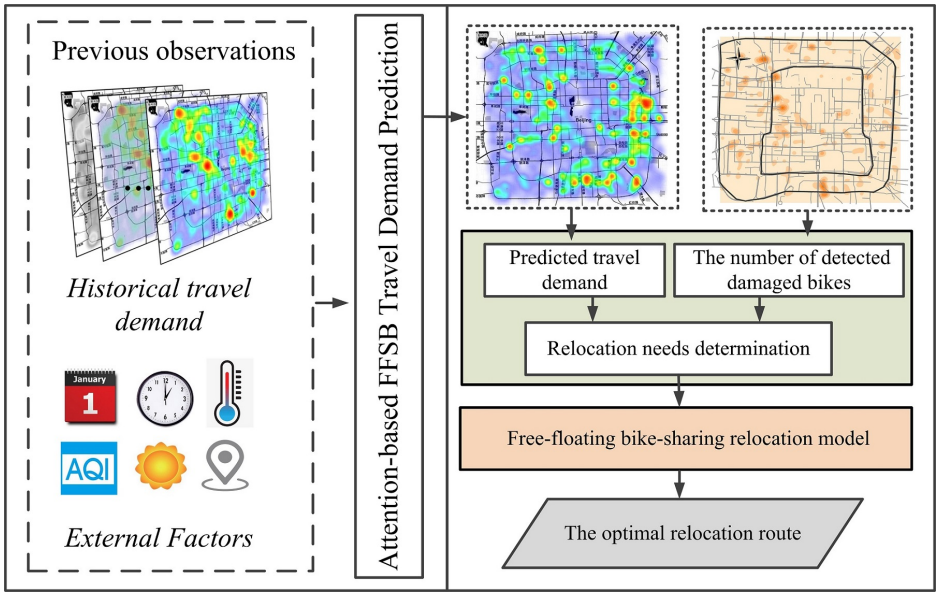

Fig.1. Architecture of the whole framework.

3.1. Attention-based FFSB travel demand prediction

3.1.1 Long Short-Term Memory network

Time series models are widely applied to the short-term demand forecasting of FFSBs as it varies with time during the day. In deep learning theory, Recurrent Neural Network (RNN) and Long Short-Term Memory (LSTM) network are developed for time series modeling. These neural networks consider both the current state and the continuous feedback between time steps to make the predictions. LSTM is developed to avoid the vanishing gradient and exploding gradient problem that can be encountered in training the traditional RNN by introducing a memory cell c_t and three gates including an input gate i_t, a forget gate f_t, and an output gate o_t, as shown in Fig. 2(a).

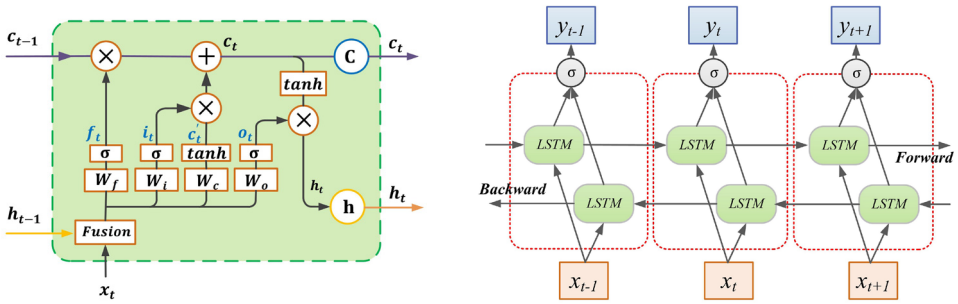

(a) (b)

Fig. 2. Architecture of (a) LSTM and (b) Bi-directional LSTM.

Input gate:

$$i_t = sigmoid(W_{ix}x_t + W_{ih}h_{t-1} + b_i) \quad (1)$$

Forget gate:

$$f_t = sigmoid(W_{fx}x_t + W_{fh}h_{t-1} + b_f) \quad (2)$$

Output gate:

$$o_t = sigmoid(W_{ox}x_t + W_{oh}h_{t-1} + b_o) \quad (3)$$

Cell state:

$$c'_t = \tanh\,(W_{cx}x_t + W_{ch}h_{t-1} + b_c) \quad (4)$$

$$c_t = f_t \circ c_{t-1} + i_t \circ c'_t \quad (5)$$

Hidden output:

$$h_t = o_t \circ tanh\,(c_t) \quad (6)$$

Activation function:

$$tan\,h(x) = \frac{e^x - e^{-x}}{e^x + e^{-x}} \quad (7)$$

$$sigmoid(x) = \frac{1}{1 + e^{-x}} \quad (8)$$

In equations (1) - (6), x_t is the input vector to the LSTM unit at time t, and h_{t-1} is the hidden state vector at time $t-1$. $W_{ix}, W_{ih}, W_{fx}, W_{fh}, W_{ox}, W_{oh}, W_{cx}$ and W_{ch} are the weight matrices of the three gates, while b_i, b_f, b_o, b_c are the corresponding bias vectors. The results of the input gate i_t and forget gate f_t are then used to calculate the current cell state c_t in Eq. (5), ensuring that the cell state is controlled by the current cell state and long-term memory. The operator $\circ$ refers to the Hadamard product, which is the scalar product of two vectors (Xu. et al, 2018; Ma. et al, 2018).

However, simply stacking multiple layers of LSTM units fails to model the characteristics of the whole input sequence when making predictions (Hao et al., 2019). Besides, the prediction accuracy of the LSTM structure would also decrease to some extent when the input sequence becomes longer, especially the unidirectional LSTM. The idea of bi-directional LSTM (Bi-LSTM) comes from bi-directional RNN (Schuster and Paliwal, 1997). The unidirectional LSTM only preserves the information of the past, therefore only information flows from backward to forward. However, in bi-directional LSTM architecture, the information can not only flow backward to forward but also from forward to backward with two separate hidden layers in Fig. 2(b). Similarly,

parameters of the forward and backward layers are updated with equations (1) - (6). It has been proved that the bi-directional networks are substantially better than unidirectional ones in short-term passenger flow prediction (Ma et al., 2018).

3.1.2 Attention-based predicting framework

The encoder-decoder architecture provides a standard approach using deep neural networks to deal with sequence-to-sequence prediction problems. The encoder process encodes the whole sequence into a fixed-length context vector through the input time steps. The decoder process then decodes this vector and makes predictions. A potential limitation of this model is that it needs to compress all the necessary information of the input sequence into a fixed-length vector, which fails to model the long-input time series data. The attention mechanism frees the fixed-length internal representation by providing a richer context c_u in the encoder-decoder architecture in Fig. 3. It helps neural networks to identify which time steps of the input are more relevant thus allowing the decoder to pay special attention, which in general speeds up the learning and lifts the skill of the model prediction (Bahdanau et al., 2014).

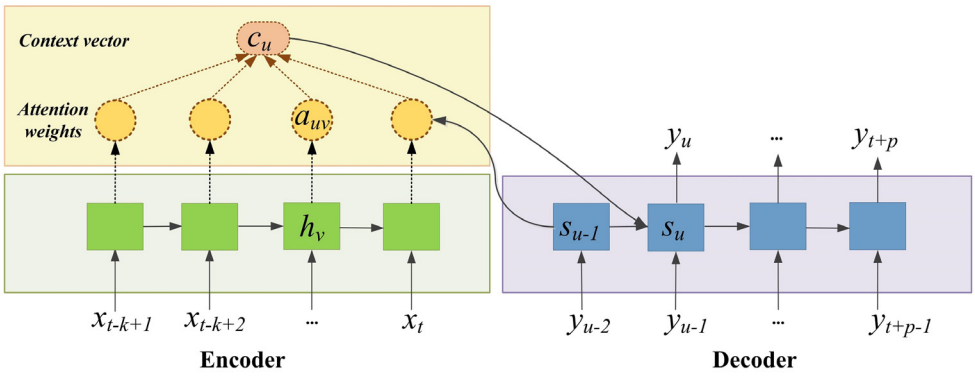

Fig. 3. Encoder-Decoder architecture with the attention mechanism.

In the attention-based architecture, the bi-directional LSTM network is selected to build the encoder network, and the LSTM network is chosen as the decoder network in Fig. 3 (Hao et al., 2019). When making the predictions for output y_u, the attention score a_{uv} specifies how much encoder hidden state h_v should be paid attention to the decoder for making predictions in Eq. (9) - (11). Eq. (10) is a Softmax function for normalizing the attention scores. k is the length of the input sequence and FC represents the fully-connected neural network to calculate the attention scores in the encoder network in Eq. (11).

$$c_u = \sum_{v=1}^{k} a_{uv} h_v \tag{9}$$

$$a_{uv} = \frac{exp\ (e_{uv})}{\sum_{v=1}^{k} exp\ (e_{uv})} \tag{10}$$

$$e_{uv} = FC(s_{u-1}, h_v) \tag{11}$$

By integrating the context vector c_u, the LSTM hidden state s_u is computed in

Eq. (12), which will be then used to predict the target y_u.

$$s_u = f(s_{u-1}, y_{u-1}, c_u) \tag{12}$$

Historical data contains valuable information for forecasting future travel demand. Nevertheless, when dealing with time-series data, different historical time steps are required with different attention. In this study, we propose a novel attention-based passenger flow (ATTPF) prediction model, which adopts the Encoder-Decoder architecture embedded with the attention mechanism to further enhance the model's prediction ability and flexibility. Besides, since bike-sharing is an outdoor travel mode, the travel demand is more susceptible to some external features, such as the day-of-week, hour-of-day, weather data (Temperature, Wind Speed), and air quality data (AQI). Multi-source data are collected dynamically and input into the ATTPF model. In detail, the historical bike-sharing travel demand is extracted by the encoder bi-directional LSTM. The external variables are fed into a full-connected neural network for feature representation learning, where the categorical variables are first converted into one-hot encoding form. A concatenate layer is used to merge the multi-source data. The fused representations are used to generate the richer context vectors, and then decode by the LSTM network to make predictions at each time step. The complete structure of the model is shown in Fig. 4.

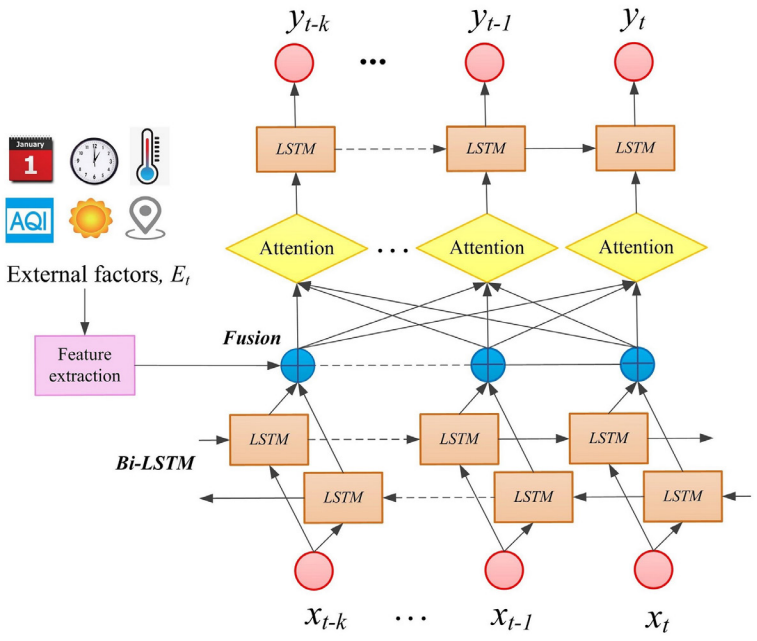

Fig. 4. Structure of the ATTPF prediction model.

3.2. A data-driven bike-sharing relocation model

3.2.1. Problem description

The operator-based FFSB relocating can be regarded as a pickup-and-delivery problem. Suppose that the bike rebalancing network is a complete directed graph $G = (V, A)$, and the vertex set $V = \{1, \ldots, n\}$ is split into non-zero imbalance zones. Due

to the fluctuating travel demand in different zones, each zone has several requests at period *t*, denoted as $q_i^t,\ i \in \{1, \dots, n\}$. The operational shared bikes collected from the pickup zones can be transferred to the delivery zones or returned to the depot by the relocation staff.

In the real-world bike-sharing relocation process, several constraints need to be considered: (1) Multiple vehicles are deployed from the depot to fulfill the relocation demand of each zone; (2) Two types of shared bikes are involved. Operational bikes are redistributed between different zones to satisfy the travel demand, while the damaged bikes should be collected and sent back to the depot for repair, therefore they cannot be relocated to other zones. Naturally, some new bikes will also be put into service at the depot and assigned to the needed zones by the relocation vehicles, which ensures the normal running of the free-floating bike-sharing system.

3.2.2. Determining the needed bike relocations

In this paper, the relocation of shared bikes is of two types: the operational bikes, and the damaged bikes. The developed ATTPF model predicts the short-term inflow and outflow of the FFSBs in each zone of a city. For the dynamic FFSB relocation, the day is separated into T periods, $t \in \{0,1, \dots, t, \dots, T\}$. For zone i, the short-term pick-up demand (outflow) and drop-off demand (inflow) at a given period t are denoted as pd_i^t and dd_i^t. Moreover, the number of available operational bikes (overstocked bikes) a_i^t and the number of damaged shared bikes b_i^t, are retrieved from the historical data. We denote s_i^t as the net flow of FFSB at zone i at period t, which is defined as the difference between the forecasted inflow dd_i^t and outflow pd_i^t in Eq. 13. The number of FFSBs needed for relocation q_i^t derives from the number of overstocked bikes at the beginning of the period a_i^t, plus the difference between the forecasted vehicle arrivals dd_i^t and bikes that were taken by clients pd_i^t in Eq.14 (Santos and Correia, 2019). Here, a safety stock of shared bikes ss_i^t for each zone is considered.

$$s_i^t = dd_i^t - pd_i^t, \qquad t \in \{0, 1, \dots, t, \dots, T\} \tag{13}$$

$$q_i^t = a_i^t - ss_i^t + dd_i^t - pd_i^t, \qquad a_i^t > 0 \tag{14}$$

The positive value of q_i^t implies that zone i is a pickup zone, in which the number of q_i^t bikes should be removed. On the opposite, the negative value of q_i^t denotes that zone i is a delivery zone, where q_i^t bikes should be supplied.

The damaged FFSBs not only affect the user's experience but also undermine the demand forecasting and relocation tasks. Therefore, it is necessary to consider both operational and damaged shared bikes relocation in the bike-sharing system. In general, when finding the nearby bikes, users unlock the FFSBs by scanning the QR code with their smartphone and start their ride. Afterward, when arriving at their destination they lock the shared bike and walk. Once the user unlocks a damaged bike, they may find this problem after riding. When this happens, the user will stop riding this bike immediately and unlock a new bike nearby. It should be noted that the users have different travel behavior when meeting the operational and damaged shared bikes. Therefore, we design an effective algorithm to discover the damaged FFSBs based on the users' travel behavior. Supposing that the same user unlocks two shared bikes in a

short time interval (e.g. less than 3 min) continuously, and the first trip distance is short (e.g., less than 200 m), we consider that the first unlocked shared bike is damaged or limited in its usage thus requiring repair. The detailed process for detecting damaged FFSBs from the historical travel records is presented in Algorithm 1.

Algorithm 1: Detection of damaged bikes in a free-floating bike-sharing system

Input: FFSB historical travel records
Initialize the parameters: pre-defined time threshold K_t, pre-defined distance threshold K_d;
Obtain the unique user ID from historical travel records $U = [u_1, u_2, \dots, u_M]$
for each user ID u_i in U:
    Obtain the trip chain TC_i of u_i from the historical travel records
    $TC_i = [TR_{i,1}, TR_{i,2}, \dots, TR_{i,N}]$; $TR_{i,j}$ is the jth travel records of u_i
    for $TR_{i,j}$ in trip chain TC_i:
        Calculate the time interval between the successive two trips
        $t_{i,j} = T_{i,j} - T_{i,j-1}$; $T_{i,j}$ is the start time of jth travel records of u_i.
        Calculate the travel distance of the successive two trips $d_{i,j-1}$ and $d_{i,j}$
        if the time interval $t_{i,j} < K_t$ and $d_{i,j-1} < K_d$ **then**
            Record the bike ID of $TR_{i,j-1}$, location of longitude and latitude
        end if
    end for
end for
Output: the damaged bikes ID and current locations

3.2.3. Formulation of the relocation model

In this section, we propose a multi-period relocation model considering the collection of damaged bikes. The notations are listed in Table 2.

Table 2. Notation in the free-floating bike-sharing relocation model

Parameters	
T	Set of periods, $t \in \{0,1, \dots, t, .., T\}$
V_t	Set of zones that need bikes or can supply bikes for relocation in period t
D_t	The departure depot set of period t
D_t'	The ending depot set of period t
A_t	Set of arcs between the zones of period t
Q	Capacity in the number of bikes of each relocation vehicle
L	The unit service time for loading or unloading a bike
d_{ij}	Dispatching distance of the relocation vehicle between zones *i* and *j*
m_i^t	Number of relocation vehicles in the depot *i* at beginning of period t
b_i^t	Number of damaged bikes at zone i at beginning of period *t*, where $b_i^t \geq 0$
q_i^t	Number of relocated operational bikes at zone i at the beginning of period *t*
ξ_i^t	Number of bikes carried in (out) from the relocation vehicle at zone i in period *t*, where $\xi_i^t = b_i^t + \lvert q_i^t \rvert$

s_i^t	Service time in zone *i* in period *t*, where $s_i^t = \xi_i^t \cdot L$
ET_i^t	The earliest service time of zone *i* in period *t*
LT_i^t	The latest service time of zone *i* in period *t*
C_d	Dispatching cost per kilometer of the relocation vehicle
C_s	Service cost of staff by carrying one bike in (out) from the relocation vehicle
C_p	Penalty for not fulfilling or delaying one relocation request
v	The travel speed of the relocation vehicle (km/h)
M	A large constant
Decision variables	
x_{ij}^t	a binary variable, taking value 1 if a relocation vehicle is moved between zones *i* and *j* in period *t*, 0 otherwise
f_{ij}^t	an integer variable, the operational bike load on the relocation vehicle traveling between zones *i* and *j* in period *t*
l_{ij}^t	an integer variable, the damaged bike load on the relocation vehicle traveling between zones *i* and *j* in period *t*
y_i^t	a binary variable, taking value 1 if zone *i* is visited in period *t*
τ_i^t	the service start time of zone *i* in period *t*

The FFSB relocation problem can be mathematically formulated as follows:

Objective function

$$Minimize \quad C_d \cdot \sum_{(i,j)\in A_t} d_{ij} \cdot x_{ij}^t + C_s \cdot \sum_{i \in V_t} \xi_i^t \cdot y_i^t + C_p \cdot \sum_{i \in V_t} \xi_i^t \cdot (1 - y_i^t) \tag{15}$$

Subject to:

$$\sum_{j\in V_t} x_{ij}^t \le m_i^t, \qquad i \in D_t \tag{16}$$

$$\sum_{i\in D_t} \sum_{j\in V_t} x_{ij}^t = \sum_{i\in D_t'} \sum_{j\in V_t} x_{ji}^t \tag{17}$$

$$\sum_{j\in V_t} x_{ij}^t - \sum_{j\in V_t} x_{ji}^t = 0, \qquad i \in V_t \tag{18}$$

$$\sum_{j\in V_t} f_{ij}^t - \sum_{j\in V_t} f_{ji}^t = q_i^t \cdot y_i^t, \qquad \forall i \in V_t \tag{19}$$

$$\sum_{j\in V_t} l_{ij}^t - \sum_{j\in V_t} l_{ji}^t = b_i^t \cdot y_i^t, \qquad \forall i \in V_t \tag{20}$$

$$\sum_{j\in V_t} x_{ij}^t - y_i^t = 0, \qquad \forall i \in V_t \tag{21}$$

$$max\{0, q_i^t, -q_j^t\} \cdot x_{ij}^t \le f_{ij}^t \le min\ \{Q, Q + q_i^t, Q - q_j^t\} \cdot x_{ij}^t, \qquad \forall (i,j) \in A_t \tag{22}$$

$$b_i^t \cdot x_{ij}^t \le l_{ij}^t \le (Q - b_j^t) \cdot x_{ij}^t, \qquad \forall (i,j) \in A_t \tag{23}$$

$$l_{ij}^t + f_{ij}^t \le Q \cdot x_{ij}^t, \qquad \forall (i,j) \in A_t \tag{24}$$

$$\xi_i^t = rb_i^t + |q_i^t|, \qquad \forall i \in V_t \tag{25}$$

$$s_i^t = \xi_i^t \cdot L, \qquad \forall i \in V_t \tag{26}$$

$$\tau_i^t - \tau_j^t + s_i^t + \frac{d_{ij}}{v} \le M \cdot \left(1 - x_{ij}^t\right), \quad \forall (i,j) \in A_t, i \ne j \tag{27}$$

$$ET_i^t \le \tau_i^t \le LT_i^t, \qquad \forall i \in V_t \tag{28}$$

$$x_{ij}^t \in \{0,1\}, \qquad \forall (i,j) \in A_t \tag{29}$$

$$y_i^t \in \{0,1\}, \qquad \forall i \in V_t \tag{30}$$

The objective function (15) minimizes the generalized cost function for this particular period t which includes: the cost of relocation vehicles dispatching, the service cost of the staff by moving the FFSBs in (out) from the relocation vehicles, and penalty for not fulfilling relocation requests. Constraints (16) restrict the number of relocation vehicles leaving depot i at the beginning of period t up to the available relocation vehicles. Constraints (17) impose all used vehicles return to the depot (or dummy depot) after completing their route at the end of period t. Constraints (18) ensure the vehicle balance restrictions. Constraints (19)-(20) ensure the operational and damaged FFSBs flow balance restrictions, respectively. In the real-world shared bikes relocation, some zones may be visited multiple times in one period. In our model, constraints (21) make some simplifications and ensure that each zone served at most once during each period. Constraints (22) impose lower and upper bounds on the operational FFSB flows on each arc by considering whether or not an arc is traveled by a relocation vehicle. For the lower bound, if the vehicle travels between zones *i* and *j* at period *t*, then f_{ij}^t should be at least greater than q_i^t if $q_i^t > 0$ (because the number of operational FFSBs q_i^t has just been collected at zone i) or greater than $-q_j^t$ if $q_i^t < 0$ (because the number of operational FFSBs q_j^t would be supplied to the next zone). Similar considerations apply to the upper bound. Constraints (23) impose lower and upper bounds on the damaged FFSB flows, which is positive bike flow value on the arc. Constraints (24) are the vehicle capacity constraints on each arc. In constraints (25), ξ_i^t is the number of shared bikes carried in (out) from the relocation vehicle at zone i at period *t*. The damaged FFSBs can only be collected and moved into the relocation vehicle. The service time s_i^t in zone *i* in period *t* is obtained in constraints (26). Constraints (27) and (28) guarantee the schedule feasibility of the relocation vehicles with respect to time considerations when visiting the zones. Constraints (29)-(30) impose binary conditions on the variables x_{ij}^t and y_i^t.

The dynamic relocation is implemented throughout the daytime and takes the real-time usage of FFSBs into account. In this paper, we adopt a multi-period optimization to handle the time-varying demand, which decomposes the dynamic process for the whole service time into well-connected static problems with a fixed duration. As shown in Fig. 5, we determine the relocation demand of each zone based on the predicted demand gap and the detected number of damaged FFSBs in each period.

The relocation problem over each period is a static problem being solved through the proposed hybrid metaheuristic algorithm. At the end of each period (except the last period), the relocation vehicles will stay at the last served zones waiting for the updated relocation routes for the next period. Both the operational bikes to be relocated as well as the damaged bikes to be collected at each zone are updated in the next period and used to determine a new routing strategy. The detailed process is as follows.

1. In the first period, the relocation vehicles depart from the depot to perform the relocation tasks. A dummy depot is created with a distance of 0 from other zones, which is the ending depot of this period. The relocation model imposes all used vehicles return to the dummy depot, but actually the vehicles would stay at the last served zones. The location of each vehicle, the load of operational and damaged bikes are stored, which are the inputs passed to the next planning period for the route decision-making.
2. In the next period, the relocated zone set V_t and the departure depot set D_t are dynamically updated to determine the new relocation routes. The starting positions of the routes are the last visiting zones with corresponding loads on each vehicle. Besides, the relocation vehicles will also depart from the depot if they are available. Some vehicles may not perform the relocation tasks during this period, and they will stay in the last served zones and wait for the relocation activities in the following periods. At the end of the period (except the last period), all used vehicles return to the dummy depot. This procedure is repeated until the end of the modeling horizon.
3. In the last period, the relocation vehicles should end at the depot. Considering that a certain number of damaged bikes are collected in the relocation vehicles in the previous periods, they need to be unloaded in the depot. On the one hand, the damaged bikes can be timely sent back to the depot for maintenance. On the other hand, the damaged bikes can be unloaded to avoid taking up too much space for the relocation of operational bikes.

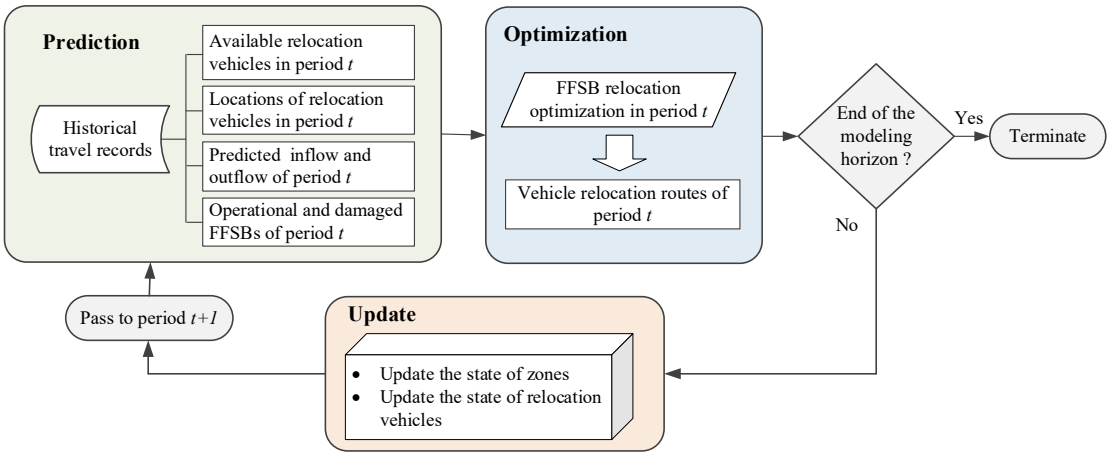

Fig. 5. Multi-period optimization approach to dynamically update data.

3.3. A hybrid metaheuristic solution approach

For the relocation route determination in each period, we propose a new hybrid metaheuristic algorithm that incorporates variable neighborhood search (VNS) and enhanced simulated annealing (ESA) algorithm to satisfy the above constraints. Variable neighborhood search (VNS) is a metaheuristic method for solving a set of combinatorial optimization and global optimization problems (Hansen, et al., 2010; Ranjbar and Saber, 2020). The proposed VNS-ESA solution approach is based on the VNS framework for the neighborhood searching phase. In Algorithm 2, the VNS-ESA approach starts with an initial solution generated by using the Clarke-Wright algorithm (Altinel and Oncan, 2005). Then, a set of neighborhood structures is generated by the shaking procedure. We develop an ESA algorithm with a modified acceptance probability for local search based on the best neighborhood from the VNS. These two algorithms are performed iteratively until reaching the determined iterative step. The role of the shaking procedure allows the algorithm to escape from the local minimum and to efficiently explore the search space. The ESA for local search is used to intensify exploration of neighborhoods around promising solutions and prevents solutions to be trapped in the local optimum.

Algorithm 2. The VNS-ESA algorithm

Input: a set of neighborhood structures N_k for $k = 1, \dots, k_{max}$ for shaking.
Generate an initial solution by using the Clarke-Wright algorithm, $s = s_0$; f is the objective function.
for $k = 1$ **to** k_{max} **do**
  Shaking procedure: pick the solution s' from the kth neighborhood $N_k(s)$;
  Local search by ESA algorithm; Find the best neighbor s'' of s';
  if local optimum s'' is better than s **then**
    $s = s''$; $k = 1$;
  otherwise $k = k + 1$;
until stopping criteria
Output: The best found solution s.

With the shaking procedure, several new neighborhood structures are generated (Hemmelmayr et al., 2009). Two exchange operators are introduced in the shaking procedure, the Cross-exchange and the iCross-exchange in Fig. 6. We use these operators to exchange nodes on the two routes in the current solution to generate the new neighborhood structures. For each shaking execution, the probability of the Cross-exchange operator being selected is larger than that of the iCross-exchange operator because the route solution is directional. The original direction of the route should be kept as much as possible during the path exchange process to increase the possibility of obtaining a feasible solution.

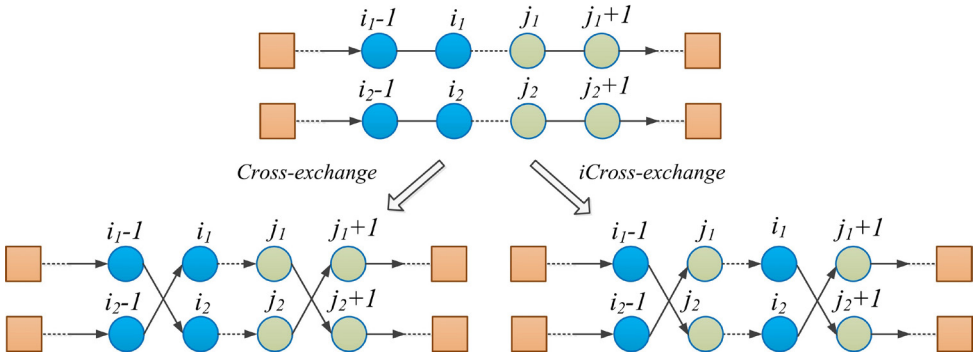

Fig. 6. The Cross-exchange and the iCross-exchange operators.

The ESA algorithm is proposed to search for the best route possible in each iteration. Simulated annealing (SA) is a probabilistic algorithm for approximating the global optimum (Kirkpatrick et al., 1983; Wei et al., 2018). SA is based on the idea of accepting the worst solutions occasionally in the hope of escaping the current local optimal solutions. Specifically, once a better neighborhood solution is identified in the search process, this movement will be accepted and the current solution will be replaced. Besides, a worse neighborhood solution would be accepted in SA with a certain probability P in Eq. (31) to avoid obtaining a local optimum. The acceptance probability consists of two parameters, T, and $\Delta cost$. T is called the temperature, which gradually reduces in the search process. $\Delta cost$ is the difference in fitness between the new solution and the current solution. The SA algorithm will stop until an adequate final temperature has been reached. In the ESA algorithm, a modified acceptance probability is proposed in Eq. (32) to prevent solutions to be trapped in local optimal solutions more effectively. Specifically, the acceptance of a new solution considers not only the gap to the current solution, $\Delta cost$, but also the gap to the optimal solution that has been reached, $\Delta cost'$.

$$P = e^{-\Delta cost/T} \tag{31}$$

$$P(ls, ls', ls_b, T) = \frac{exp\ (-\Delta cost/T)}{exp\ (-\Delta cost'/T)} \tag{32}$$

where $\Delta cost = f(ls') - f(ls)$; $\Delta cost' = f(ls_b) - f(ls')$; ls is the current solution; ls' is the neighbor solution; ls_b is the current best solution; $f()$ is the objective function in Eq. (15). The procedure of the ESA algorithm is summarized in Algorithm 3.

In the ESA algorithm, a new feasible solution ls' is generated through the local search operators, which is used to intensify exploration of neighborhoods around promising solutions. The 2-exchange operator is executed by exchanging the positions of the two visited zones in the initial tour, in Fig. 7 (a) (Hernando et al., 2011). The 2-opt method is designed to find a route that crosses over itself and reorders it, which includes eliminating and reconnecting two edges in a different way to obtain a new feasible route, as is shown in Fig. 7(b) (Muren et al., 2019). In addition, not all zones can be served within a period, so we remove some zones in the current routes and add the unserved zones with a certain probability. For each iteration of the local search process, we randomly choose one operator, which can fully utilize the operators' search

capabilities and expand the search space to some extent. The present VNS-ESA algorithm is numerically compared with the high-performance commercial solver (CPLEX 12.10) and other heuristics with small-scale examples in Appendix A. Results show that the VNS-ESA algorithm can obtain better solutions compared with the SA and VNS algorithm in a reasonable time.

Algorithm 3: The ESA algorithm

Initialize the ESA control parameter: initial temperature T_0, cooling rate λ, the initial solution s' with the neighborhood $N_k(s)$ from the VNS.
Set $T = T_0$; $ls = s'$; $cost = f(ls)$; $f(ls_b) = f(s')$; f is the objective function.
while termination criterion is not satisfied **do**
  for number of new solutions:
    Select a feasible solution ls' with the Local Search operator
    $\Delta cost = f(ls') - f(ls)$
      if $\Delta cost < 0$ **then**
        $cost_{new} = f(ls')$; $ls = ls'$
        if $f(ls') < f(ls_b)$ **then**
          $f(ls_b) = f(ls')$; $ls_b = ls'$
        end if
      else
        $\Delta cost' = f(ls_b) - f(ls')$
        $p = \dfrac{exp\,(-\Delta cost/T)}{exp\,(-\Delta cost'/T)}$
        generate a random number, $\delta \in (0,1)$
        if $\delta < p$ **then**
          $cost_{new} = f(ls')$; $ls = ls'$
        else
          $cost_{new} = f(ls)$
        end if
      end if
    $cost = cost_{new}$
    Decrease the temperature periodically: $T = \lambda \times T$
  end for
end while
Set $s'' = ls$
Output: the optimized route in the local search process s''

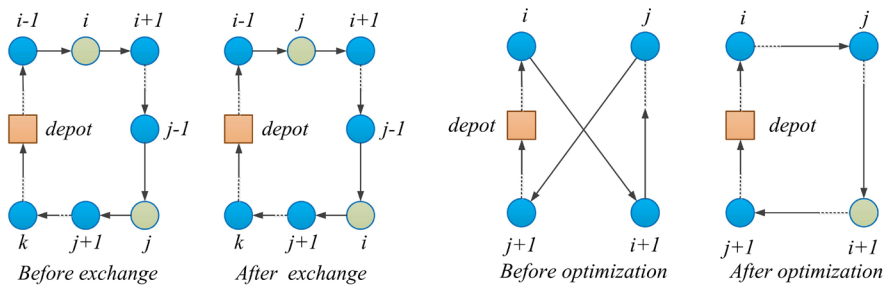

(a) (b)

Fig. 7. The schematic diagram of (a) 2-exchange operator and (b) 2-opt operator.

4. Case-study application to real-world FFSBs

4.1. Free-floating bike-sharing data

This study analyzes the FFSB data collected by Mobike in Beijing. A total of 992,183 travel records are recorded from May 10th to May 24th, 2017, each of which contains the bike ID, user ID, travel time, longitude, and latitude. The study area is located within the 3rd ring road of Beijing. Due to the characteristic that FFSBs are scattered across the city without docking stations, the research area is partitioned into 729 grids (basic research zones) with a grid-size of 500 m in Fig. 10. We assume that the time for users to find FFSBs in the basic research zones can be ignored. To make the users find the FFSBs within a short distance and efficiently rebalance the FFSBs among different zones, it is necessary to control the size of the grids.

4.2. Spatial and temporal trip patterns

We aggregate the FFSB trips by hours of the week to analyze the temporal usage patterns in Fig. 8. Overall, the larger bike-sharing trip volume appears on weekdays than on weekends (Du et al., 2019; Chang et al., 2020). The travel demand on weekdays demonstrates a triple-peak nature related to commuting trips. However, on weekends, the FFSB travel demand is reduced to a large extent, and the rush hours become less pronounced.

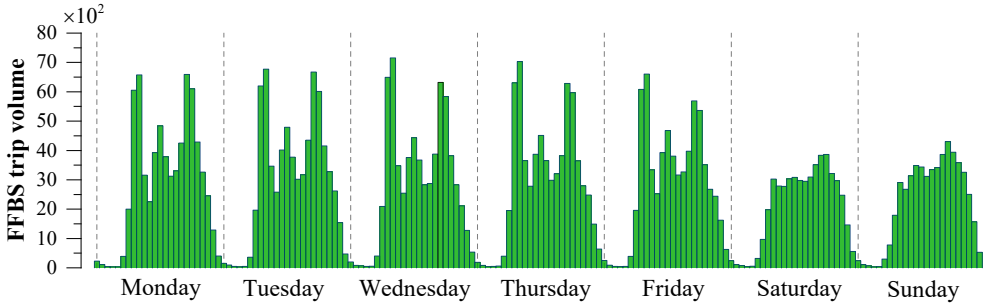

Fig. 8. FFSB travel demand aggregated to hours of the week.

The spatial trip volume distribution of FFSB on weekdays is shown in Fig. 9. In the morning, a large amount of FFSB travel demand emerges at the edge of the 3rd ring road, which is mostly around the residential communities. Later, a lot of trips aggregate in restaurants and shopping malls in the downtown area at noon. In the evening, people

travel by FFSBs from the companies in the city center to the residential areas in the city fringe. As a whole, fluctuating spatial and temporal travel demand of FFSBs exists among different areas of the city during the day.

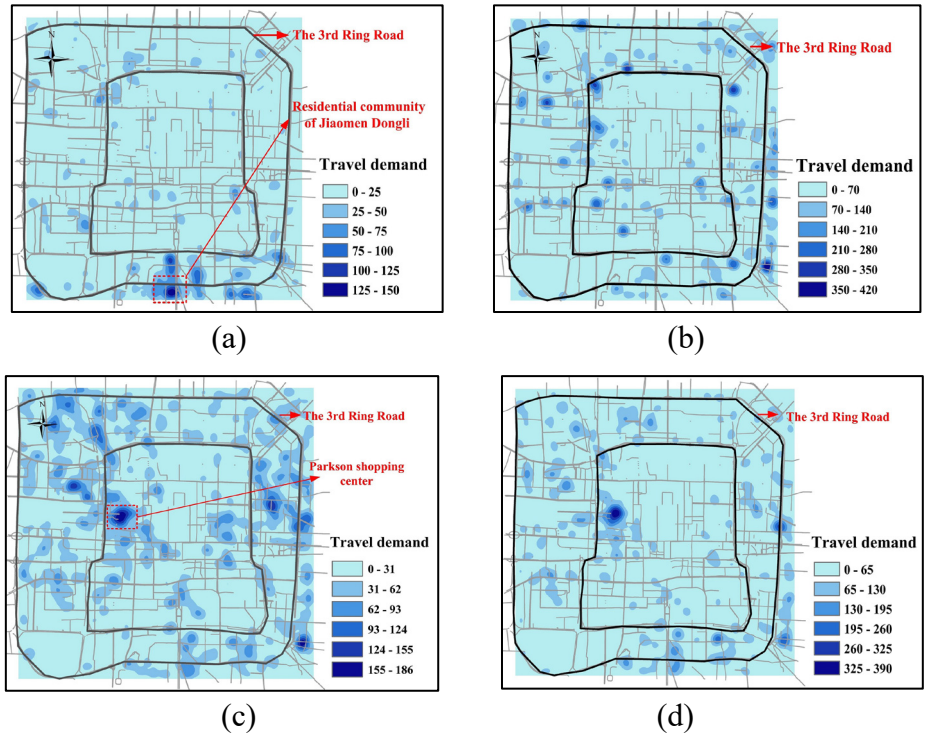

Fig. 9. The spatial and temporal distribution of FFSBs on weekdays: (a) 6:00-7:00; (b) 8:00-9:00; (c) 12:00-13:00; and (d) 18:00-19:00.

Fig. 10 shows the net flow volume of FFSBs in the selected 729 grids based on Eq. (13). It can be seen that the net flow distribution fluctuates during the daytime. In peak hours, a large demand gap exists in different regions. The role of each grid (pickup zone or delivery zone) varies with time. For example, in zone A, more outflow trips appear in the morning peak hours in Fig.10 (a). Therefore, there is a need to transfer FFSBs to this zone. However, in the evening peak in Fig.10 (c), the inflow trips are larger than the outflow trips, and overstock FFSBs exist during this period, where some shared bikes need to be moved to other zones. Besides, the relocation needs are varying in other zones such as zone B and C. To better satisfy the users' needs, considerable efforts should be carried out properly for dynamic rebalancing the shared bikes.

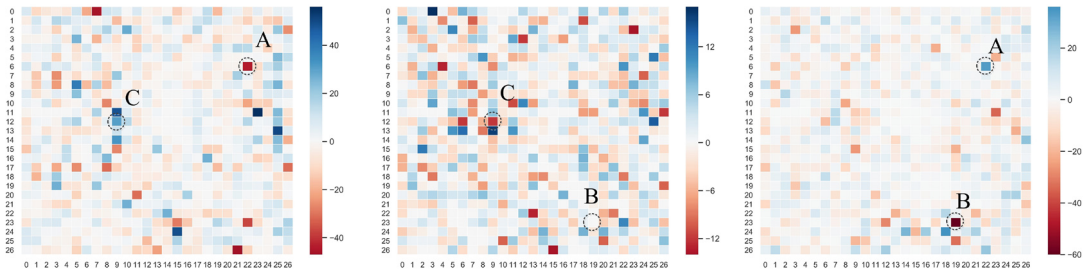

Fig.10. Net flow distribution of FFSB trips on weekdays: (a) 8:00-9:00; (b) 12:00-13:00; and (c) 18:00-19:00.

4.3. The damaged FFSB distributions

Adopting algorithm 1 in section 3.2.2, we detect the potentially damaged FFSBs in the free-floating bike-sharing system. According to a survey near the Hujialou subway station in Beijing (Beijing Youth Daily news, 2017), fifty shared bikes are randomly selected to test the damaged bike rate of FFSBs. Among them, there were three FFSBs that had different types of problems and could not be used for a ride. Therefore, the damaged bike rate in this survey is calculated as 6.00%. In our experiment, the value of K_t and K_d are set as 5 minutes and 200 meters respectively, which means that the same user unlocks two different shared bikes in 5 minutes continuously, and the first trip distance is less than 200 meters. Thus we can get the distribution of damaged FFSBs in Fig.11. The number of discovered damaged FFSBs is 830, and a total of 14,446 FFSBs have been used in the study area according to the historical travel records. Therefore, the calculated damaged bike rate is 5.75%. We then map the discovered damaged shared bikes to the corresponding zones according to their locations. Notably, we cannot guarantee that each discovered bike is damaged, but there is a high probability that they are unusable. Therefore, these potentially damaged bikes are worthy of being collected and moved to the depot for further examination and repair. To obtain more effective parameter settings, we can conduct more practical surveys for the damaged bike rate. The smaller the values of K_t and K_d are set, the greater the probability that the detected FFSBs are damaged. These parameters can be determined according to actual needs.

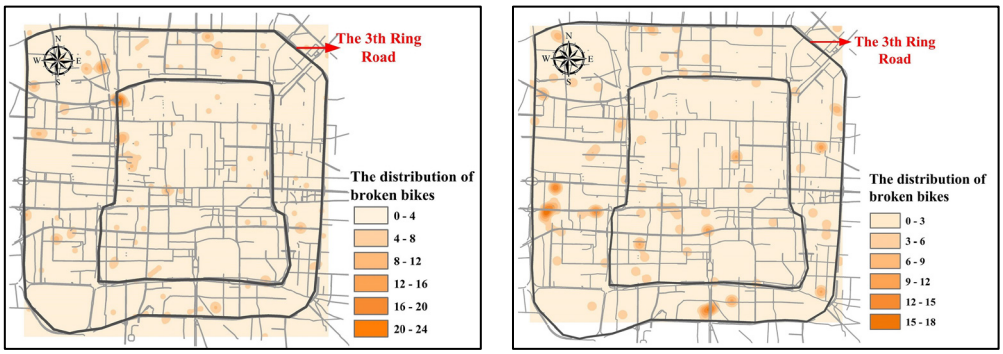

(a) (b)

Fig. 11. The distribution of damaged shared bikes on (a) weekday and (b) weekend discovered from the historical travel records.

5. Method application

5.1. Predictive performance of the proposed ATTPF model

The proposed ATTPF model is applied for short-term FFSB inflow and outflow prediction in the selected 749 zones. Besides, 80% of the data is used as the training set and the remaining 20% is used as the test set. The input historical inflow and outflow data are normalized to the interval [0, 1]. For categorical variables such as the time-of-day and day-of-week, we convert them into the one-hot encoding form in the data processing stage.

Five baseline methods are used to test the predictive performance of the ATTPF model, including historical average (HA), autoregressive integrated moving average

(ARIMA), support vector regress (SVR), gated recurrent unit (GRU), and LSTM. The HA and ARIMA (Ahmed and Cook, 1979) are the widely-used statistical methods. The SVR (Jiang et al., 2014), GRU (Ji and Hou, 2017), and LSTM are the recently developed artificial intelligence algorithms. Root mean squared error (RMSE) and mean absolute error (MAE) are selected as the measurement metrics in Eq. (33) and (34). $y^{(i)}$ and $\widehat{y^{(i)}}$ are the true and predicted inflow/outflow in the ith time interval. n is the size of the test set.

$$\mathrm{RMSE} = \sqrt{\frac{1}{n}\sum_{i=1}^{n}(y^{(i)} - \widehat{y^{(i)}})^2} \tag{33}$$

$$\mathrm{MAE} = \frac{1}{n}\sum_{i=1}^{n}\left|y^{(i)} - \widehat{y^{(i)}}\right| \tag{34}$$

Table 3 shows the performance comparison of the proposed ATTPF model and other baseline methods for inflow and outflow prediction. It can be seen that the ATTPF model obtains the best prediction performance under almost all evaluation metrics. For the 1-hour outflow forecasting task, compared with the ARIMA, SVR, GRU, and LSTM models, the RMSE of the ATTPF model is reduced by 40.86%, 17.74%, 32.21%, and 22.37% respectively. The computation time of the different models is compared. Although the HA model can make predictions in a short time, the forecast error is large. The proposed ATTPF model requires a longer training time than LSTM and GRU models due to the encoding and decoding process and the attention mechanism. In general, the proposed ATTPF model can be trained within a reasonable time, and effectively achieve the short-term prediction task.

Table 3. Predictive performance comparison on different time intervals.

Model	1-hour			2-hour			3-hour		
	RMSE	MAE	Time (s)	RMSE	MAE	Time (s)	RMSE	MAE	Time (s)
(a) inflow prediction									
HA	7.73	4.74	0.11	10.86	7.68	0.10	11.52	7.74	0.06
ARIMA	5.10	3.76	204.26	10.06	7.28	99.79	12.39	8.21	39.37
SVR	4.79	2.96	20.32	6.11	4.50	10.02	7.79	6.86	7.88
GRU	6.51	3.88	363.45	7.89	5.47	172.71	10.44	7.81	117.73
LSTM	4.49	3.15	325.34	5.83	4.10	196.54	6.78	6.20	135.20
ATTPF	**3.65**	**2.46**	396.484	**4.98**	**3.82**	234.17	**5.87**	**4.56**	162.01
(b) outflow prediction									
HA	6.95	4.59	0.12	9.02	6.65	0.10	11.77	7.79	0.08
ARIMA	6.51	4.53	197.70	11.41	8.5	117.50	16.11	9.38	41.46
SVR	4.68	2.71	19.88	5.63	4.00	10.63	6.97	5.07	8.67
GRU	5.68	3.43	369.06	7.65	5.23	186.47	9.68	7.17	108.09
LSTM	4.96	3.20	346.69	5.47	4.13	191.52	6.91	6.28	138.18
ATTPF	**3.85**	**2.63**	423.21	**4.86**	**3.66**	227.37	**5.62**	**4.43**	150.13

The ablation studies are performed on 1-hour time interval with the inflow and outflow datasets in Table 4. We compare the predictive performance of the ATTPF framework with multi-source data. The ATTPF-T only uses the historical trip data. Based on the ATTPF-T model, the ATTPF-TW, ATTPF-TA, and ATTPF-TE further fuse the weather variables (Weather state, Temperature, Wind Speed), air quality data (AQI), external variables (day-of-week, hour-of-day) respectively. As expected, the ATTPF-ALL model combines all the above components and variables, which leads to considerable improvement in prediction accuracy. Therefore, all these variables contribute to improving the prediction accuracy of FFSB travel demand. We choose two typical zones A and B to show the predicted values and actual values in Fig. 12, where their geographical locations can be found in Fig. 10.

Table 4. Ablation studies of the proposed ATTPF model on the 1-hour time interval.

Model	inflow prediction		outflow prediction	
	RMSE	MAE	RMSE	MAE
LSTM	4.49	3.15	4.96	3.20
ATTPF-T (with trip data)	4.32	3.01	4.72	3.04
ATTPF-TW (with trip and weather data)	4.05	2.82	4.02	2.74
ATTPF-TA (with trip and air quality data)	4.28	2.98	4.56	3.01
ATTPF-TE (with trip and external data)	4.23	2.95	4.39	2.88
ATTPF-ALL (with full data)	**3.65**	**2.46**	**3.85**	**2.63**

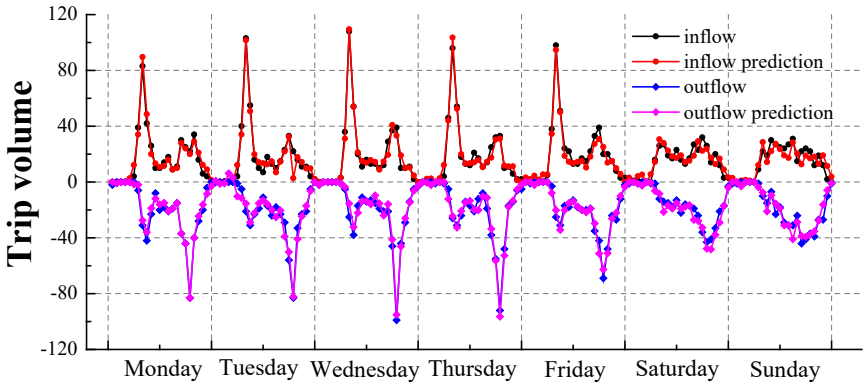

(a)

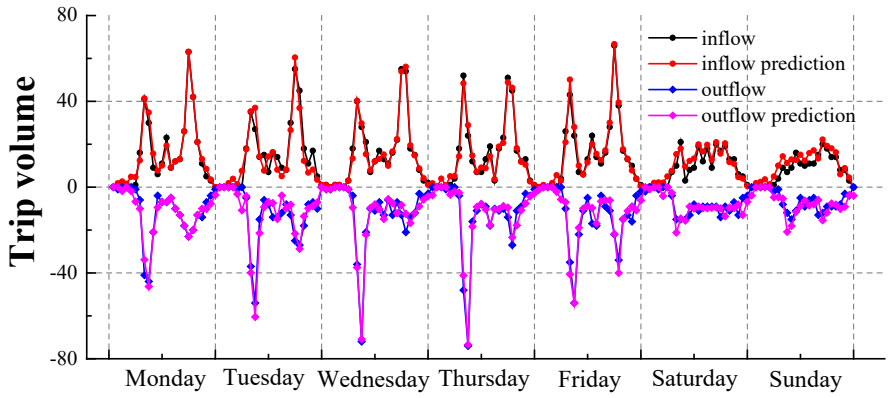

(b)

Fig. 12. The visualization results for 1-hour prediction of the inflow and outflow: (a) zone A; (b) zone B.

5.2. Real-world relocation optimization

For the real-world case study of bike relocation in Beijing, the whole city is divided into different areas. Each area is equipped with a depot, which stocks many operational shared bikes used for relocation tasks. The relocation vehicles and staff start from the depot at the beginning of the day to perform the assigned tasks. Considering the practical factors, e.g. the size of the divided zone and the speed of the relocation vehicles, the surrounding zones have been arranged to be relocated by the corresponding depot. In this paper, the research area within the 3rd ring road in Beijing is partitioned into 729 zones with a grid-size of 500 m. In the divided zones, we assume that there are 4 shared bike depots, which are located in the center of each service area in Fig.13. For example, depot 1 is responsible for the shared bike relocation tasks in the green zones. Besides, the detected damaged bikes are assigned to the corresponding zones before the dynamic relocation process.

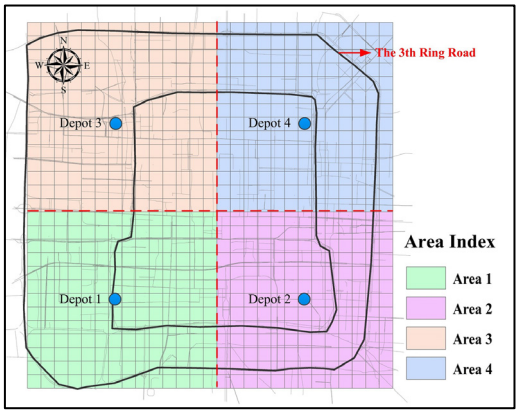

Fig. 13. The location of the zones and depots in the study area.

The operators drive vehicles for FFSBs relocation during the daytime (i.e., 8:00 - 18:00). The time interval for dynamic relocation can be 1 hour, 2 hours, 3 hours, etc., which divides the day into several periods. In this paper, we set the length of each period to 1 hour in Table 5. In the first period, multiple relocation vehicles depart from the

depot to perform the relocation tasks. At the end of the period (except the last period), the relocation vehicles will stay at the last served zones waiting for the updated relocation routes, and then start to perform the relocation tasks in the next period. In the last period, all relocation vehicles should end at the depot. Considering that the damaged bikes are collected in the relocation vehicles in the previous periods, they need to be timely unloaded in the depot. Thus, we set the relocation vehicles should return to the depot at end of period 5 and period 10. The dispatching cost of the relocation vehicle is $C_d = 0.7\ \$/km$. We suppose the service cost is $C_s = 0.05\ \$$ for the staff moving one bike in (out) from the relocation vehicle and the unit service time is $L = 2\ s$. The load capacity Q of the relocation vehicle is set as 100. The travel distance between the centroids of each zone can be calculated according to their actual locations. The travel speed of the relocation vehicle is $v = 35\ km/h$, referring to the average vehicle speed of Beijing in 2017 (Sohu News, 2018). The penalty for not fulfilling or delaying one relocation request C_p is set to 3. At the beginning of the day, we assume that there are 4 vehicles in each depot that can be used for relocation.

Table 5 presents the detailed optimized relocation results in different periods on the weekday (May 15, 2017), which includes the number of relocated zones, the number of relocation vehicles used, the relocation distance cost, the total staff service cost, the penalty cost, and the service rate. The service rate refers to the ratio of the FFSBs that have been served to the FFSBs that need to be served. Note that we do not consider the zones where the total relocation demand is less than 5 in our case study because the limited relocation resources (vehicles and staff) should be assigned to zones in urgent need of relocation. The models are solved by the hybrid metaheuristic algorithm VNS-ESA. In the morning, noon, and evening peak hours, the relocation demand is higher than that in other periods. More vehicles and staff need to be arranged for these relocation tasks, which leads to the increased expenses for both distance costs and staff service costs. For example, in Area 2, 64 zones are in urgent need of relocation in period 1 starting from the depot, while there are only 35 zones that should be served in period 3. Among the four service areas, more zones in Area 3 need to be served on weekdays with higher relocation needs, especially on morning and evening peak hours. Besides, some zones cannot be served with the initial 4 vehicles in each depot. For example, the service rate of Area 3 is 0.83 in period 5 and is 0.76 in period 10. On the one hand, some zones are with the high relocation demand. On the other hand, the collection of damaged FFSBs occupy the capacity of the relocation vehicle. Thus, these vehicles should return to the depot after a few periods.

Table 5. Performance indicators in four selected areas for different periods.

Period	1 (8:00-9:00)	2 (9:00-10:00)	3 (10:00-11:00)	4 (11:00-12:00)	5 (12:00-13:00)	6 (13:00-14:00)	7 (14:00-15:00)	8 (15:00-16:00)	9 (16:00-17:00)	10 (17:00-18:00)
(a) Area 1										
Number of relocated zones	53	26	32	65	59	41	30	47	42	75
Number of relocated damaged bikes	5	3	7	11	7	3	2	5	3	4
Number of relocation vehicles	4	4	4	4	4	4	4	4	4	4
Distance cost ($)	59.48	26.18	32.66	43.93	36.71	45.80	38.10	45.33	47.20	43.26

Staff service cost ($)	34.55	6.90	8.75	15.00	12.35	11.75	7.55	12.20	13.30	22.90
Penalty cost ($)	0	0	0	219	255	0	0	0	0	513
Service rate	1	1	1	0.87	0.84	1	1	1	1	0.74
(b) Area 2										
Number of relocated zones	64	40	35	64	52	34	36	32	43	64
Number of relocated damaged bikes	11	4	2	3	2	6	2	1	4	6
Number of relocation vehicles	3	4	4	4	4	3	4	4	4	4
Distance cost ($)	57.06	39.41	37.33	60.16	46.85	40.60	34.52	33.26	44.70	40.67
Staff service cost ($)	39.65	17.05	9.45	16.95	15.60	11.15	12.95	9.80	14.55	24.50
Penalty cost ($)	0	0	0	294	0	0	0	0	0	393
Service rate	1	1	1	0.84	1	1	1	1	1	0.85
(c) Area 3										
Number of relocated zones	83	47	23	55	62	51	39	42	55	77
Number of relocated damaged bikes	8	8	2	5	4	4	6	1	2	6
Number of relocation vehicles	4	4	4	4	4	3	4	4	4	4
Distance cost ($)	55.53	47.99	20.96	49.19	33.69	50.78	40.99	43.25	50.85	45.81
Staff service cost ($)	44.20	15.70	5.70	22.70	17.85	19.35	13.40	12.55	21.30	21.90
Penalty cost ($)	585	0	0	0	330	0	0	0	0	501
Service rate	0.81	1	1	1	0.83	1	1	1	1	0.76
(d) Area 4										
Number of relocated zones	78	53	25	33	40	36	21	31	47	58
Number of relocated damaged bikes	9	2	3	3	0	3	2	1	4	5
Number of relocation vehicles	4	4	4	4	4	3	4	4	4	4
Distance cost ($)	57.95	49.46	28.47	35.62	34.67	40.54	18.26	32.47	43.82	39.27
Staff service cost ($)	29.55	23.40	7.45	10.45	12.35	13.45	5.40	8.80	17.05	14.80
Penalty cost ($)	240	0	0	51	105	0	0	0	0	276
Service rate	0.88	1	1	0.97	0.95	1	1	1	1	0.84

Fig.14 compares the relocation result of Area 2 in different periods on weekdays (May 15, 2017) and weekends (May 21, 2017). The total relocation cost on weekends is less than that on weekdays. For example, during the day, the total relocation cost of Area 2 is 606.21 $ on weekdays that contains 434.56 $ for the distance cost and 171.65 $ for the staff service cost, while it reduces to 494.44 $ on weekends. During the three high-demand peaks of the working day, staff service cost accounts for a larger proportion of the total relocation cost, e.g., 40.99% during 8:00-9:00 and 37.59% during 17:00-18:00 in Fig.14 (a), because more relocation tasks need to be completed at this time interval. On weekends, the proportion of staff service cost is reduced and does not fluctuate much at different periods of the day in Fig.14 (d). There are fewer zones that need relocation and lower relocation demand due to the decreasing commuting trips. Therefore, the total relocation distance and the vehicle used for relocation are less than that on weekdays. Besides, higher relocation demand appears on weekend afternoons. For example, 42 zones need to be relocated during 15:00-16:00 in Fig.14 (e), while only 32 zones should be visited during the same period on weekdays in Fig.14 (b).

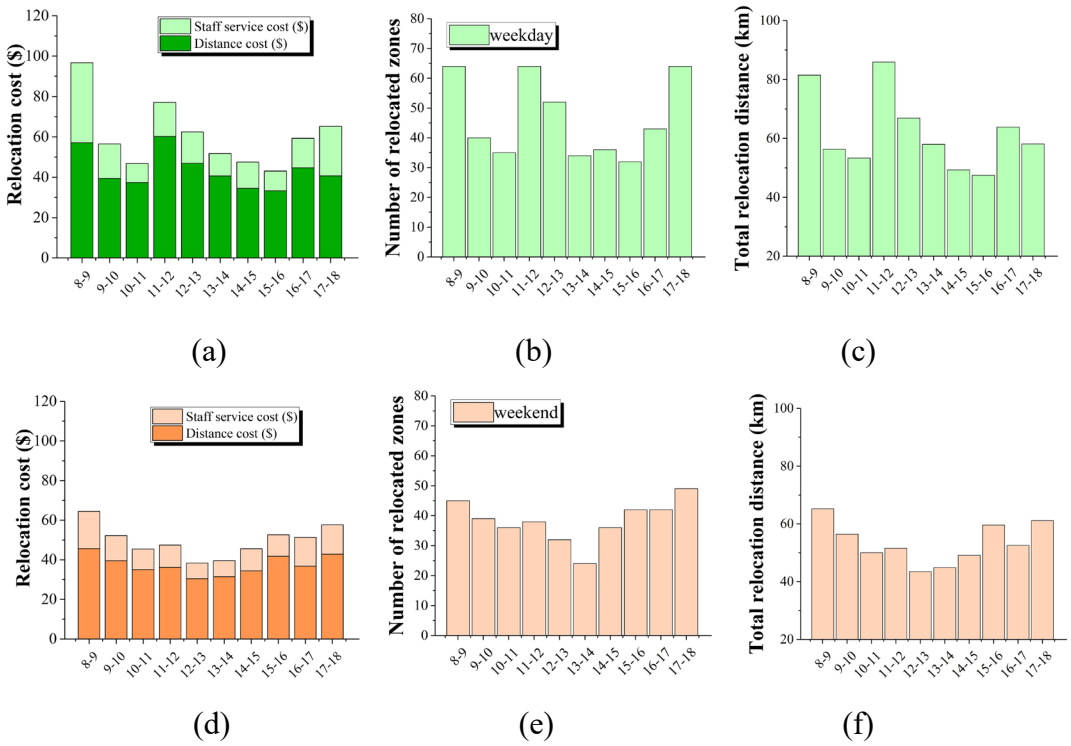

Fig. 14. The relocation result of Area 2 on weekdays and weekends: (a) Relocation cost, weekday; (b) Number of relocated zones, weekday; (c) Total relocation distance, weekday; (d) Relocation cost, weekend; (e) Number of relocated zones, weekend; (f) Total relocation distance, weekend.

In the daily FFSB relocation process, the companies should have different strategies to deal with various conditions. For example, if high relocation demand appears in the morning peak hours, the relocation vehicle may only consider the operational shared bikes relocation to alleviate the imbalance that has occurred instead of collecting damaged bikes. It is urgent at those times of the day to focus on providing bikes to clients where they are undersupplied. Table 6 presents the detailed optimized relocation results in Area 2 on weekends (May 21, 2017) with two strategies (Strategy 1: relocated operational and damaged FFSBs; Strategy 2: only relocated operational FFSBs). For different relocation strategies, it could be observed that considering the operational bike and damaged bike relocation increases the value of the daily relocation costs, including both the travel distance cost and the staff service cost. In detail, only relocating the operational bikes in special time periods, the total relocation cost and staff service cost can be reduced. For example, in Table 6, if both the operational bikes and damaged bikes are relocated in period 1 (Strategy 1), the distance cost is 45.66 $. However, only considering the operational bike relocation (Strategy 2), the distance cost is reduced to 39.45 $. Since in some zones, there are only relocation needs for damaged bikes. Strategy 2 can be adopted with urgent relocation of operational bikes, which can be effective for relocating in peak hours. Moreover, the damaged bikes can be optionally collected when the relocation tasks are not heavy. During non-peak hours, few relocation tasks exist with adequate relocation resources, e.g, in period 3 and period 7. At this time, the collection of damaged bikes should be considered without increasing much of the relocation cost, which will enhance the service level of the bike-sharing

system and timely decrease the probability of users finding damaged bikes in the system.

Table 6. Performance indicators for different relocation strategies in Area 2.

Period	1 (8:00-9:00)	2 (9:00-10:00)	3 (10:00-11:00)	4 (11:00-12:00)	5 (12:00-13:00)	6 (13:00-14:00)	7 (14:00-15:00)	8 (15:00-16:00)	9 (16:00-17:00)	10 (17:00-18:00)
(a) Strategy 1: relocated operational and damaged FFSBs										
Number of relocated operational bikes	361	243	200	212	150	155	213	206	282	275
Number of relocated damaged bikes	15	10	8	14	8	8	10	11	8	21
Number of relocated zones	45	39	36	38	32	24	36	42	42	49
Distance cost ($)	45.66	39.79	36.35	36.45	33.20	31.43	34.42	40.65	36.64	41.15
Staff service cost ($)	18.80	12.65	10.40	11.30	7.90	8.15	11.15	10.85	14.50	14.80
(b) Strategy 2: only relocated operational FFSBs										
Number of relocated operational bikes	361	243	200	212	150	155	213	206	282	275
Number of relocated damaged bikes	0	0	0	0	0	0	0	0	0	0
Number of relocated zones	35	32	36	28	25	24	36	33	42	39
Distance cost ($)	39.45	35.19	36.26	31.35	26.75	31.43	34.42	35.10	36.45	35.31
Staff service cost ($)	18.05	12.15	10.00	10.60	7.50	7.75	10.65	10.30	14.10	13.75

6. Conclusions

In the emerging free-floating bike-sharing system, shared bikes are permitted to be parked at any proper positions without the capacity problem of docking stations. However, free-floating shared bikes (FFSB) are unevenly distributed in different city regions, and the damaged bikes tend to be abandoned casually in the street, which occupies public space. Therefore, in addition to rebalancing operational bikes among different zones by multiple relocation vehicles to satisfy the users' fluctuant travel demand, there is the need to collect the damaged bikes to the depots.

This paper proposes a data-driven modeling framework for dynamic relocation in the free-floating bike-sharing system considering the collection of the damaged bikes. First of all, we investigate the spatiotemporal mobility patterns of the FFSB at a citywide scale and analyze the travel demand fluctuations that lead to the imbalance between FFSBs demand and supply. Secondly, the ATTPF model utilizing deep learning algorithms is established to forecast the short-term inflow and outflow of shared bikes in the different zones, which adopts the Encoder-Decoder architecture embedded with the attention mechanism to further enhance the model's prediction ability and flexibility. To handle the dynamic nature of the FFSB relocation, the multi-period optimization approach breaks down the dynamic process into a set of periods with a fixed duration. For each period, the relocation demand of operational bikes is determined and the damaged bikes are detected according to a method based on users' travel behavior. Then, a data-driven optimization model is proposed to formulate the problem of relocating both the operational and damaged bikes simultaneously. The new hybrid metaheuristic algorithm that incorporates enhanced simulated annealing (ESA) algorithm and variable neighborhood search (VNS) is used for route design optimization.

Small-scale numerical examples indicate that the VNS-ESA algorithm outperforms the benchmark algorithms to generate high-quality solutions within reasonable computing times. A series of real-world cases are conducted based on the Beijing FFSB data for the large-scale relocation optimization. Relocating both operational and damaged bikes will lead to higher relocation costs. It is effective to only relocate the operational bikes during peak hours with limited relocation resources. Future studies should integrate the dynamic FFSB repositioning models with multiple depots, multiple visits, and multi-objective functions, considering user satisfaction and company revenues. Moreover, more effective algorithms in reinforcement learning should be developed for the large-scale real-world relocation to improve the service level in the free-floating bike-sharing system.

Appendix A. Illustrative numerical examples

In this section, we compare the proposed hybrid metaheuristic VNS-ESA algorithm with a high-performance commercial solver, i.e., CPLEX (12.10 Academic Version) and other heuristics with the designed illustrative numerical examples. The experiments have been conducted on a PC with an Intel Core i7, 2.8 GHz CPU, and 8 GB RAM.

The experiments with different parameters are designed in Table A.1. The instance index, i.e., Z-O-D, denotes the total numbers of zones, the number of operational FFSBs needed for relocation, and the number of discovered damaged bikes respectively. The operational FFSBs demand and damaged bikes are randomly distributed in different numerical examples. The dispatching cost of the relocation vehicle is $C_d = 0.7\ \$/km$. We suppose the service cost is $C_s = 0.05\ \$$ for the staff moving one bike in (out) from the relocation vehicle. The load capacity Q of the relocation vehicle is set as 30. The travel speed of the relocation vehicle is $v = 35\ km/h$. The parameters of SA and ESA algorithms are set as follows. In these experiments, the algorithms use an initial temperature $T_0 = 10^4$, and a cooling rate of $cr = 0.005$. Table A.1 presents the comparison of the result among CPLEX, SA, VNS, ESA, and the proposed hybrid metaheuristic algorithm VNS-ESA. The option parameters of the CPLEX solver are set to default values, and the maximum time for solving the model is limited to 3000 seconds in the examples. For the heuristic methods, each instance runs 10 times to compute the average objective value, the best objective value within the same CPU time. We use the improvement of the average objective value produced by the VNS-ESA algorithm against the other three heuristic methods in percentage.

When dealing with small-scale instances, such as 5-20-5 and 10-40-10, SA, VNS, and the VNS-ESA algorithm can obtain the best possible route. With the expansion of instance scale, e.g., more zones and FFSBs needed to be relocated, it takes a longer time to get the optimal solutions. By enhancing the acceptance probability, the proposed ESA algorithm provides high-quality solutions compared with the basic SA for all instances. The shaking operation in VNS-ESA generates more neighborhood structures for diversification of the search, and thus obtains better solutions than the ESA algorithm. We can see that for all 14 instances, the VNS-ESA algorithm can yield high-quality solutions, which perform better than the CPLEX and other heuristics, especially for large-scale instances.

Table A.1. Comparison of the results of the CPLEX, SA, VNS, ESA, and the VNS-ESA algorithm.

Instance Z-O-D	CPU/s	SA		VNS		ESA		VNS-ESA		CPLEX		VNS-ESA vs SA	VNS-ESA vs VNS	VNS-ESA vs ESA
		Mean	Best	Mean	Best	Mean	Best	Mean	Best	Best	CPU/s	Improvement	Improvement	Improvement
5-10-0	5	16.21	16.21	16.21	16.21	16.21	16.21	16.21	16.21	16.21	0.10	0	0	0
5-20-5		17.21	17.21	17.21	17.21	17.21	17.21	17.21	17.21	17.21	0.32	0	0	0
10-20-5	8	25.43	24.99	26.57	24.99	25.32	24.99	24.99	24.99	24.99	0.48	1.73%	5.95%	1.30%
10-40-10		26.96	26.25	27.66	26.25	26.56	26.25	26.25	26.25	26.25	0.61	2.63%	5.10%	1.17%
20-40-10	30	38.27	36.90	38.08	37.11	38.15	36.71	36.07	35.70	35.70	6.85	5.75%	5.28%	5.45%
20-60-15		40.55	38.63	39.41	38.27	39.00	37.75	37.21	36.95	36.95	18.16	8.24%	4.69%	4.59%
30-60-15	80	48.14	47.48	51.26	47.81	47.23	45.43	44.62	44.38	44.38	39.55	7.31%	12.95%	5.53%
30-80-20		60.22	59.67	65.39	61.19	56.54	51.82	51.89	47.80	47.80	42.77	13.83%	20.65%	8.22%
40-80-20	150	58.10	55.70	65.32	63.07	55.34	54.87	53.32	52.11	52.11	113.18	8.23%	18.37%	3.65%
40-100-25		60.94	59.86	73.08	67.84	58.21	55.41	56.57	55.16	55.16	156.83	7.17%	22.59%	2.82%
50-100-25	190	61.33	59.42	81.33	79.31	59.08	56.72	57.53	56.01	55.87	1434.70	6.20%	29.26%	2.62%
50-120-30		64.61	62.57	91.28	87.35	60.86	60.07	57.59	57.23	56.96	1623.05	10.87%	36.91%	5.37%
60-120-30	280	77.20	74.72	115.36	108.76	72.28	70.25	70.36	70.25	-	>3000	8.86%	39.01%	2.66%
60-140-35		81.80	76.62	119.69	115.30	76.17	74.75	72.30	72.18	-	>3000	11.61%	39.59%	5.08%

We define the service rate as the ratio of the FFSBs that have been served to the FFSBs that need to be served. Fig. A.1 (a) and (b) show the changes of generalized cost and service rate with different settings of penalty cost C_p for not fulfilling one relocation request in the example of 40 zones. The service rate gradually increases with the larger penalty cost C_p. When there is only one relocation vehicle, due to the limitation of the vehicle capacity, the maximum service rate can only reach 0.3 in Fig. A.1 (a), so the penalty cost for not fulfilling the relocation request is larger, which leads to the higher generalized cost. The service rate gradually increases with more relocation vehicles. When there are 4 vehicles available for relocation, all the relocation needs can be satisfied. At this time, the generalized cost is mainly the cost for relocation vehicles dispatching between zones and the service cost of the staff by moving the FFSBs in (out) from the relocation vehicles at different zones. In addition, with 4 relocation vehicles available for relocation, not all the relocation needs will be met when the penalty cost C_p is set to a small value. In some zones with small relocation needs but long relocation distance, the distance cost is much greater than the penalty cost, and thus the relocation vehicles will not choose to serve those zones, resulting in a low service rate. However, when the penalty cost C_p is set to a larger value, the vehicles will visit more zones to meet the relocation needs as much as possible.

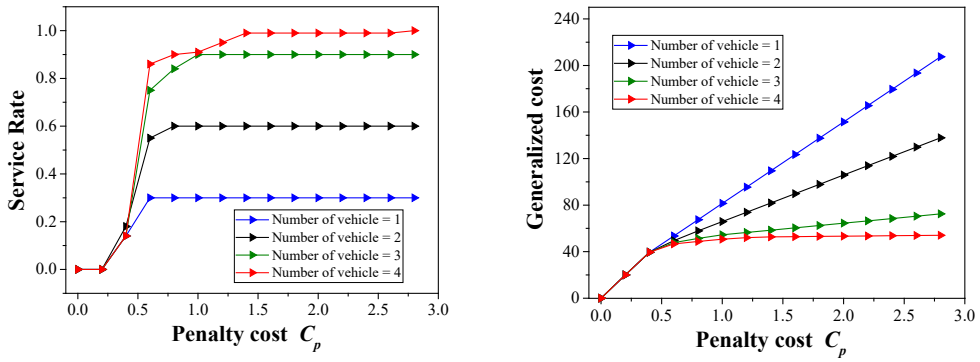

(a) (b)

Fig. A.1. The changes of service rate and generalized cost under different settings of penalty cost.

Fig. A.2 shows the changes of generalized cost and service rate with different numbers of zones and vehicles when the penalty cost is set to 3. In Fig. A.2 (a), we assume that there are 2 relocation vehicles available. With the increased number of zones, the service rate gradually decreases, and the generalized cost continues to increase, where the penalty cost accounts for a large part. Fig. A.2 (b) shows the changes of service rate and generalized cost with the different number of vehicles in the example of 40 zones. The service rate gradually increases with sufficient relocation vehicles.

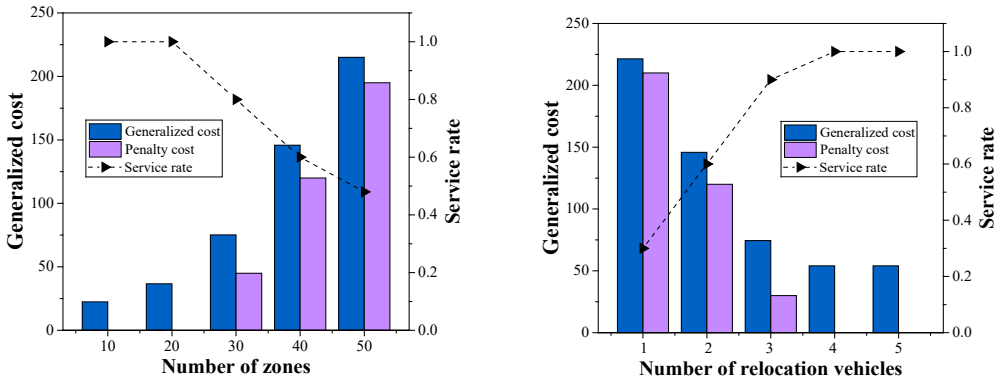

(a) (b)

Fig. A.2. The changes of service rate and generalized cost under different settings of parameters. (a) Number of zones; (b) Number of relocation vehicles.

The multi-period optimization approach is adopted to divide the dynamic FFSB relocation into well-connected static problems. The day is separated into T periods, $t \in \{0, 1, \dots, t, \dots, T\}$, and the model is solved for T times to dynamically plan the relocation activities throughout the day. At the beginning of each period t, we update the number of vehicles available in the depot, the locations and the remaining capacity of the vehicles, the number of operational and damaged bikes that need to be relocated (in section 3.2.2). Based on this information, the model is solved with the commercial solver (e.g., CPLEX) or heuristic algorithm (e.g., VNS-ESA) to determine the vehicle relocation routes in period t. The optimal solution for period t is passed for the next period planning.

Reference

Ahmed, M.S., Cook, A.R., 1979. Analysis of freeway traffic time-series data by using Box-Jenkins techniques. Transportation Research Record: Journal of the Transportation Research Board. 722, 1-9.

Altinel, I. K., Oncan, T., 2005. A new enhancement of the Clarke and Wright savings heuristic for the capacitated vehicle routing problem. Journal of the Operational Research Society. 56, 954-961.

Alvarez-Valdes, R., Belenguer, J. M., Benavent, E., 2016, Optimizing the level of service quality of a bike-sharing system. Omega - The International Journal of Management Science. 62, 163-175.

Angeloudis, P., Hu, J., Bell, M. G. H., 2014. A strategic repositioning algorithm for bicycle-sharing schemes. Transportmetrica A: Transport Science. 10(8), 759-774.

Ashqar, H. I., Elhenawy, M., Almannaa, M. H., Ghanem, A., Rakha, H. A., House, L., 2017. Modeling bike availability in a bike-sharing system using machine learning. In: Proceedings of the 5th IEEE International Conference on Models and Technologies for Intelligent Transportation Systems (MT-ITS), Naples, 374-378.

Barabonkov, D., D'Alonzo, S., Pierre, J., Kondor, D., Zhang, X., Tien, M. A., 2020. Simulating and Evaluating Rebalancing Strategies for Dockless Bike-Sharing Systems. arXiv:2004.11565.

Bahdanau, D., Cho, K., Bengio, Y., 2014. Neural machine translation by jointly learning to align and translate. arXiv preprint arXiv:1409.0473.

Beijing Youth Daily news, "The intact rate of shared bikes in Beijing should b e no less than 95%" September, 2017. [Online]. Available: http://www.cnr.cn/bj/jrbj/20170920/t20170920_523957058.shtml

Caggiani, L., Camporeale, R., Ottomanelli, M., Szeto, W., 2018. A modeling framework for the dynamic management of free-floating bike-sharing systems. Transportation Research Part C: Emerging Technologies. 87, 159-182.

Chang, X., Wu, J., He, Z., Li, D., Sun, H., Wang, W., 2020. Understanding user's travel behavior and city region functions from station-free shared bike usage data. Transportation Research Part F: Traffic Psychology and Behaviour. 72, 81-95.

Chang, X., Wu, J., Sun, H., Wang, G., Feng, Z., Bao, X., 2021. Understanding and predicting short-term passenger flow of station-free shared bike: A spatiotemporal deep learning approach. IEEE Intelligent Transportation Systems Magazine. doi: 10.1109/MITS.2021.3049362.

China daily News, "Rides on shared bikes returning to normal amid the epidemic in Beijing," April, 2020. [Online]. Available: https://www.chinadaily.com.cn/a/202004/01/WS5e848834a310128217283b73.html

Dell'Amico, M., Hadjicostantinou, E., Iori, M., Novellani, S., 2014. The bike sharing rebalancing problem: Mathematical formulations and benchmark instances. Omega-The Internationa Journal of Management Science. 45, 7-19.

Du, Y., Deng, F., Liao, F. 2019. A model framework for discovering the spatio-temporal usage patterns of public free-floating bike-sharing system. Transportation Research Part C: Emerging Technologies. 103, 39-55.

Du, M., Cheng, L., Li, X., Tang, F., 2020. Static rebalancing optimization with considering the collection of malfunctioning bikes in free-floating bike sharing

system. Transportation Research Part E: Logistics and Transportation Review. 141,102012.

Fournier, N., Christofa, E., Knodler, M., 2017. A sinusoidal model for seasonal bicycle demand estimation. Transportation Research Part D: Transport and Environment. 50, 154-169.

Hao, S., Lee, D., Zhao, D., 2019 Sequence to sequence learning with attention mechanism for short-term passenger flow prediction in large-scale metro system. Transportation Research Part C: Emerging Technologies. 107, 287-300.

Hansen, P., Mladenović, N. Moreno Pérez, J.A., 2010.Variable neighbourhood search: methods and applications. Annals of Operations Research, 175, 367-407.

He, S., Shin, K., 2020. Towards Fine-grained Flow Forecasting: A Graph Attention Approach for Bike Sharing Systems. In: Proceedings of the Web Conference 2020 (WWW '20), New York, USA, 88-98.

Heitz, C., Etschmann, R., Stoeckle, R., Bachmann, T., Templ, M., 2018. User-based Redistribution in Free-floating Bike Sharing Systems. In: Proceedings of 2018 Annual International Conference of the German Operations Research Society (GOR), Brussels, Belgium, 12-14, 555-562.

Hemmelmayr, V. C., Doerner, K. F., Hartl, R. F., 2009. A variable neighborhood search heuristic for periodic routing problems. European Journal of Operational Research, 195(3), 791-802.

Hernando, L., Pascual, J.A., Mendiburu, A., Lozano, J., 2011. A study on the complexity of TSP instances under the 2-exchange neighbor system. In: Proceedings of IEEE Symposium on Foundations of Computational Intelligence (FOCI), Paris, 15-21.

Ho, S.C., Szeto, W.Y., 2014. Solving a static repositioning problem in bike-sharing systems using iterated tabu search. Transportation Research Part E: Logistics and Transportation Review. 69, 180–198.

Ho, S. C., Szeto, W. Y., 2017. A hybrid large neighborhood search for the static multi-vehicle bike-repositioning problem. Transportation Research Part B: Methodological, 95, 340–363.

Huo, X., Wu, X., Li, M., Zheng, N., Yu, G., 2020. The allocation problem of electric car-sharing system: A data driven approach. Transportation Research Part D: Transport and Environment. 78, 102192.

Ji, J., Hou, J., 2017. Forecast on Bus Trip Demand Based on ARIMA Models and Gated Recurrent Unit Neural Networks. In: Proceedings of international Conference on Computer Systems, Electronics and Control (ICCSEC), Dalian, China, 105-108.

Jiang, X., Zhang, L., Chen, X., 2014. Short-term forecasting of high-speed rail demand: A hybrid approach combining ensemble empirical mode decomposition and gray support vector machine with real-world applications in China. Transportation Research Part C: Emerging Technologies. 44, 110-127.

Kadri, A. A., Kacem, I., Labadi, K., 2016. A branch-and-bound algorithm for solving the static rebalancing problem in bicycle sharing systems. Computers & Industrial Engineering. 95, 41–52.

Kirkpatrick, S., Gelatt, C.D., Vecchi, M.P., 1983. Optimization by simulated annealing. Science. 220, 671-680.

Laporte, G., Meunier, F., Calvo, R. W., 2018. Shared mobility systems: an updated

survey. Annals of Operations Research, 271(1), 105-126.
Legros, B., 2019. Dynamic repositioning strategy in a bike-sharing system; how to prioritize and how to rebalance a bike station. European Journal of Operational Research. 272(2), 740-753.
Li, H., Zhang, Y., Ding, H., Ren, G., 2019. Effects of dockless bike-sharing systems on the usage of the London Cycle Hire. Transportation Research Part A: Policy and Practice. 130, 398-411.
Lin, L., He, Z., Peeta, S., 2018. Predicting Station-level Hourly Demand in a Large-scale Bike-sharing Network. Transportation Research Part C: Emerging Technologies. 97, 258-276.
Liu, A., Szeto, W.Y., Ho, S., 2018. A static free-floating bike repositioning problem with multiple heterogeneous vehicles, multiple depots, and multiple visits. Transportation Research Part C: Emerging Technologies. 92, 208-242.
Liu, Y., Liu, Z., Jia, R., 2019. DeepPF: A deep learning based architecture for metro passenger flow prediction. Transportation Research Part C: Emerging Technologies. 101, 18-34.
Lu, H., Zhang, M., Su, S., Gao, X., Luo, C., 2019. Broken Bike Recycling Planning for Sharing Bikes System. IEEE Access. 7, 177354-177361.
Ma, X., Zhang, J., Du, B., Ding, C., Sun, L., 2018. Parallel Architecture of Convolutional Bi-Directional LSTM Neural Networks for Network-Wide Metro Ridership Prediction. IEEE Transactions on Intelligent Transportation Systems. 20 (6), 2278-2288.
Ma, X., Zhang, X., Li, X., Wang, X., Zhao, X., 2019. Impacts of free-floating bike sharing system on public transit ridership. Transportation Research Part D: Transport and Environment. 76, 100-110.
Ma, X., Ji, Y., Yuan, Y., Oort, N., Jin, Y., Hoogendoorn, S., 2020. A comparison in travel patterns and determinants of user demand between docked and dockless bike-sharing systems using multi-sourced data. Transportation Research Part A: Policy and Practice.139, 148-173.
Muren, Wu, J., Zhou, L., Du, Z., Lv, Y., 2019. Mixed steepest descent algorithm for the traveling salesman problem and application in air logistics. Transportation Research Part E: Logistics and Transportation Review. 126, 87-102.
Pal, A., Zhang, Y., 2017. Free-floating bike sharing: Solving real-life large-scale static rebalancing problems. Transportation Research Part C: Emerging Technologies, 80, 92-116.
Pan, L., Cai, Q., Fang, Z., Tang, P., Huang, L., 2019. A Deep Reinforcement Learning Framework for Rebalancing Dockless Bike Sharing Systems. In: Proceedings of the AAAI Conference on Artificial Intelligence, 33(01), 1393-1400.
Pfrommer, J., Warrington, J., Schildbach, G., 2014. Dynamic vehicle redistribution and online price incentives in shared mobility systems. IEEE Transactions on Intelligent Transportation Systems. 15(4), 1567-1578.
Ranjbar, M., Saber, R. G., 2020. A variable neighborhood search algorithm for transshipment scheduling of multi-product at a single station. Applied Soft Computing, 106736.
Regue, R., Recker, W., 2014. Proactive vehicle routing with inferred demand to solve the bikesharing rebalancing problem. Transportation Research Part E: Logistics and

Transportation Review. 72, 192-209.
Santos, G., Correia, G., 2019. Finding the relevance of staff-based vehicle relocations in one-way carsharing systems through the use of a simulation-based optimization tool. Journal of Intelligent Transportation Systems. 23(6), 583-604.
Schuster, M., Paliwal, K. K., 1997. Bidirectional recurrent neural networks. IEEE Transactions on Signal Processing. 45(11), 2673–2681.
Shui, C. S., Szeto, W. Y., 2018. Dynamic green bike repositioning problem – A hybrid rolling horizon artificial bee colony algorithm approach. Transportation Research Part D: Transport and Environment. 60, 119-136.
Shui, C. S., Szeto, W. Y., 2020. A review of bicycle-sharing service planning problems. Transportation Research Part C: Emerging Technologies, 117, 102648.
Sina News, "Totaled 2.2 Million Bikes in Bike-Sharing System in Beijing," February, 2018. [Online]. Available: https://news.sina.cn/gn/2018-02-12/detail-ifyrkrva7577336.d.html?pos=3&vt=4
Sohu News, "The number of days of severe traffic congestion in Beijing decreased by 9%, and vehicle speed increased by 10% in 2017," January, 2018. [Online]. Available: https://www.sohu.com/a/219919883_745330
Sohrabi, S., Paleti, R., Balan, L., Cetin, M., 2020. Real-time prediction of public bike sharing system demand using generalized extreme value count model. Transportation Research Part A: Policy and Practice.133, 325-336.
Solomatine, D., Ostfeld, A., 2008. Data-driven modeling: some past experiences and new approaches. Journal of Hydroinformatics, 10(1), 3-22.
Sun, Z., Li, Y., Zuo, Y., 2019. Optimizing the location of virtual stations in free-floating bike-sharing systems with the user demand during morning and evening rush hours. Journal of advanced transportation, 2019(1), 1-11.
Szeto, W.Y., Liu, Y., Ho, S.C., 2016. Chemical reaction optimization for solving a static bike repositioning problem. Transportation Research Part D: Transport and Environment. 47, 104–135
Szeto, W. Y., Shui, C. S., 2018. Exact loading and unloading strategies for the static multi-vehicle bike repositioning problem, Transportation Research Part B: Methodological. 109, 176–211.
Usama, M., Zahoor, O., Bao, Q., Liu, Z., Shen, Y., 2019a. Dockless Bike-Sharing Rebalancing Problem with Simultaneous Faulty Bike Recycling. In: Proceedings of 19th COTA International Conference of Transportation Professionals, 4963-4974.
Usama, M., Shen, Y., Zahoor, O., 2019b. A free-floating bike repositioning problem with faulty bikes. Procedia Computer Science, 151, 155-162.
Usama, M., Zahoor, O., Shen, Y., Bao, Q., 2020. Dockless bike-sharing system: Solving the problem of faulty bikes with simultaneous rebalancing operation. Journal of Transport and Land Use, 13(1), 491-515.
Wang, B., Kim, I., 2018. Short-term prediction for bike-sharing service using machine learning. Transportation Research Procedia. 34, 171-178.
Wang, Y., Szeto, W. Y., 2018. Static green repositioning in bike sharing systems with broken bikes. Transportation Research Part D: Transport and Environment. 65, 438–457.
Wei, L., Zhang, Z., Zhang, D., Leung, S., 2018. A simulated annealing algorithm for the capacitated vehicle routing problem with two-dimensional loading constraints.

European Journal of Operational Research. 265, 843–859.
Xu, C., Ji, J., Liu, P., 2018. The station-free sharing bike demand forecasting with a deep learning approach and large-scale datasets. Transportation Research Part C: Emerging Technologies. 95, 47-60.
Yoon, J. W., Pinelli, F., Calabrese, F., 2012. Cityride: A Predictive Bike Sharing Journey Advisor. 2012. In: Proceedings of IEEE 13th International Conference on Mobile Data Management, Bengaluru, Karnataka, 306-311.
Zhang, D., Yu, C., Desai, J., Lau, H.Y.K., Srivathsan, S., 2017. A time-space network flow approach to dynamic repositioning in bicycle sharing systems. Transportation Research Part B: Methodological. 103, 188-207.
Zhai, Y., Liu, J., Du, J., Wu, H., 2019. Fleet size and rebalancing analysis of dockless bike-sharing stations based on markov chain. International Journal of Geo-Information, 8(8), 334.